A COMPLETE SAMPLE OF MEGAPARSEC-SIZE DOUBLE RADIO SOURCES FROM SUMSS

L. Saripalli,[1] R. W. Hunstead,[2] R. Subrahmanyan[1] and E. Boyce,[2,3]

ABSTRACT

We present a complete sample of megaparsec-size double radio sources compiled from the Sydney University Molonglo Sky Survey (SUMSS). Almost complete redshift information has been obtained for the sample. The sample has the following defining criteria: Galactic latitude $|b| > 12.^{\circ}5$, declination $\delta < -50^{\circ}$ and angular size $> 5'$. All the sources have projected linear size larger than 0.7 Mpc (assuming $H_o = 71$ km s^{-1} Mpc^{-1}). The sample is chosen from a region of the sky covering 2100 square degrees. In this paper, we present 843-MHz radio images of the extended radio morphologies made using the Molonglo Observatory Synthesis Telescope (MOST), higher resolution radio observations of any compact radio structures using the Australia Telescope Compact Array (ATCA), and low resolution optical spectra of the host galaxies from the 2.3-m Australian National University (ANU) telescope at Siding Spring Observatory. The sample presented here is the first in the southern hemisphere and significantly enhances the database of known giant radio sources. The giant radio sources with linear size exceeding 0.7 Mpc have an abundance of (215 Mpc)$^{-3}$ at the sensitivity of the survey. In the low redshift universe, the survey may be suggesting the possibility that giant radio sources with relict lobes are more numerous than giant sources in which beams from the centre currently energize the lobes.

Subject headings: Surveys – samples: galaxies – radio galaxies: continuum – optical spectra

---

[1]CSIRO Australia Telescope National Facility, Locked bag 194, Narrabri NSW 2390, Australia. Lakshmi.Saripalli@csiro.au and Ravi.Subrahmanyan@ csiro.au

[2]School of Physics, University of Sydney, NSW 2006, Australia. rwh@physics.usyd.edu.au

[3]MIT Kavli Institute, 77 Massachusetts Avenue, Cambridge MA 02139. eboyce@mit.edu

1. Introduction

Double radio sources of large linear size—the giant radio sources—form a valuable resource for understanding the radio galaxy phenomenon and probing the intergalactic medium (Subrahmanyan & Saripalli 1993). Their large sizes raise several interesting questions, not only concerning their formation but also issues related to the long lifetime of their nuclear beam activity and jet stability. The long timescales involved also imply that the radio structures of these giant radio sources might show evidence of changes in nuclear activity that might be linked to recent merger events or other triggers of central engine activity. Recent discoveries of radio sources with inner double structures embedded within more relaxed outer diffuse lobes (Subrahmanyan et al. 1996; Schoenmakers et al. 2000a; Saripalli et al. 2002, 2003) have drawn attention to the phenomenon of restarting in beams. Investigations into these issues clearly benefit from having large numbers of giant radio sources and, importantly, samples with uniform selection criteria.

The number of known giant radio sources has grown largely from serendipitous discoveries over the years. However, there have been several attempts in the last decade to make directed searches for these large objects. Low-frequency radio surveys with high surface brightness sensitivity are specially suited for the purpose of detecting giant radio sources. Cotter et al. (1996) presented a sample of giant radio sources selected from the 7C survey. The Westerbork Northern Sky Survey (WENSS; Rengelink et al. (1997)) was used by Schoenmakers et al. (2001) to compile a complete flux-density limited sample of giant radio sources. Lara et al. (2001) and also Machalski et al. (2001) compiled samples of large angular-size sources using the NRAO Very Large Array sky survey (NVSS; Condon et al. (1998)) and the Faint Images of the Radio Sky at Twenty cm (FIRST; Becker et al. (1995)) and worked towards identifying giant radio sources in these surveys. In this paper we describe a similar effort that has resulted in the formation of a complete sample of giant radio sources in the southern hemisphere based on the Sydney University Molonglo Sky Survey (SUMSS).

The SUMSS has been described in detail elsewhere (Bock et al. 1999; Mauch et al. 2003). The 843-MHz SUMSS was started in 1997 and uses the upgraded Molonglo Observatory Synthesis Telescope (MOST) as the survey instrument. With a synthesized beam of FWHM $45\mathrm{cosec}|\delta| \times 45$ arcsec^2 at a position angle 0°, an rms noise level of ~ 1 mJy beam^{-1} and excellent spatial frequency coverage, the survey is one of the most sensitive to date for extended sources. The sample presented in this paper is from the region observed up to the end of February 2000 and covers 2100 square degrees. In Section 2 we describe the methodology adopted for initially selecting candidate giant radio sources in this sky region. Subsequently, we carried out high resolution Australia Telescope Compact Array (ATCA) radio observations for detecting radio cores in these candidates and this is reported in Sec-

tion 3. Spectroscopy of the optical identifications made at the locations of the radio cores is presented in Section 4. The resulting giant radio source sample is presented along with notes on individual sources in Section 5. In Section 6 we discuss the sample properties. The candidates that were rejected while forming the complete sample are discussed in Appendix A.

Giant radio sources are usually defined in the literature to be double radio sources with projected linear size greater than 1 Mpc; this limit was based on a Hubble constant of $H_o = 50$ km s^{-1} Mpc^{-1}. We adopt a flat cosmology with Hubble constant $H_o = 71$ km s^{-1} Mpc^{-1} and matter density parameter $\Omega_m = 0.27$. Double radio sources with linear size exceeding $0.7h_{71}^{-1}$ Mpc are large enough to be atypical and most of the extended radio structure would lie well outside of gas associated with the host galaxy; however, there is no reason for adopting a definitive linear-size cutoff apart from having well defined sample selection criteria. For consistency with previous work, we have chosen to include in our final sample all radio galaxies with linear sizes larger than 0.7 Mpc for our adopted H_o.

2. The SUMSS giant radio source candidates

Boyce (2000) examined the sky area covered by SUMSS prior to 2000 February for candidate giant radio sources; at that time SUMSS was 26% complete. Boyce also limited the search to declinations $\delta < -50^\circ$ and Galactic latitudes $|b| > 12\overset{\circ}{.}5$. A total of 2100 square degrees of sky area was examined by eye. At the low frequency of 843 MHz and the low resolution of $\approx 45''$, the lobes rather than cores or hotspots of extragalactic double radio sources dominate the images. A search was made for single connected structures that have a large angular size, close pairs of extended radio components—double sources that appeared to be extended along the line joining the two components—and any triple sources. The angular extent was estimated to be the separation between the peaks of the outermost components and only sources with angular size exceeding $5'$ were deemed to be candidate giant radio sources. A total of 35 candidates were selected as potential giant radio sources.

In this paper we adopt a nomenclature for sources that identifies the survey and their giant nature. The giant radio sources that satisfied the selection criteria are given the prefix: SGRS (SUMSS giant radio source), and the remainder of the candidate list are given the prefix: SGRSC (SUMSS giant radio source candidate). It may be noted that some of the candidates in the Appendix have linear sizes exceeding 0.7 Mpc and are giant radio sources, some are double radio sources with smaller linear size and some candidates are composed of unrelated components.

Twelve extended double radio sources (SGRSC J0020−7321, J0129−6433, J0200−6007,

J0534−8203, J0551−5655, J0603−5429, J0622−5938, J1959−6402, J2150−6210, J2222−5617, J2228−5600 and J2253−5813) were detected in the search area with angular sizes, measured from the SUMSS images, that were close to the limit of $5'$ and below the angular-size cutoff. We included them in follow-up high-resolution radio imaging to test whether there were any giant radio sources among them. As discussed below, the follow-up observations revealed that some of these double/triple components were unrelated sources and some had linear sizes smaller than 0.7 Mpc.

For the two sources SGRC J0143−5431 and J0326−7730 the emission peak in one of the lobes was displaced well away from the edge, unlike the other candidates. For these two sources we identified components representing the extended emission with a Gaussian fit to a slice along the lobe. The angular extent for the sources were estimated using these identified components.

The selection criteria included a declination limit so that the SUMSS radio images and the follow-up with the E-W ATCA had synthesized beams that were not too elongated. Low Galactic latitudes were avoided to facilitate optical identifications. The lower limit of $5'$ on the angular size was chosen to include essentially all powerful edge-brightened double radio sources in the nearby universe with total linear size larger than 0.7 Mpc and to ensure that the candidate list did not overwhelm our resources for radio/optical follow-up; this criterion was the same as that adopted by Schoenmakers et al. (2001). The angular-size cutoff, together with the sensitivity limit of the survey, potentially discriminates against edge-darkened (FR-I type) double radio sources; even if the largest angular size in edge-darkened sources exceeds $5'$, it is possible that the separation between the peaks in their lobes is less than this cutoff and such sources might be missed. Effectively, this criterion implies almost a factor of two larger linear-size cutoff for FR-I sources in any redshift bin.

For the adopted cosmology, the selection criteria imply that our giant radio source sample will be complete for redshifts $z \leq 0.13$: all edge-brightened giant sources with linear size exceeding 0.7 Mpc are detectable within the corresponding 3.5×10^7 Mpc^3 comoving volume. At redshifts exceeding 0.13, only sources with progressively larger linear size would be selected. Powerful double radio sources with edge-brightened structure have radio power exceeding about 1.3×10^{25} W Hz^{-1} at 843 MHz, corresponding to the FR-I/FR-II break power (Owen & Ledlow 1994). In our adopted cosmology such sources would be detectable in SUMSS with flux density exceeding 0.3 Jy if they are at redshifts $z \leq 0.13$.

3. ATCA radio observations of the candidate list

We observed the candidate list of 35 large angular-size sources at higher resolution using the ATCA for the purpose of detecting compact radio cores that could guide the optical identification process. The ATCA observations were also aimed at examining the compact structures in the individual components as a means of identifying cases where the close components were independent sources or chance alignments.

All 35 sources were observed in 24-hr observing sessions using the 6A and 6D E-W array configurations of the ATCA during 2001 November–December (Table 1). The multi-channel continuum observations were made in the 20-cm band using a pair of 128-MHz bands centered at 1344 and 1440 MHz. Every source was observed at 4 or 5 widely spaced hour angles, each of about 6-min duration. The data were reduced in MIRIAD using an automated script with parameters optimized for imaging point sources. Multi-frequency synthesis was used to make a combined image using the data from the two adjacent frequencies; the images had beam FWHM in the range 5″–10″. The rms noise in the deconvolved images varied between 0.2–1.0 mJy beam^{-1}; the images were dynamic-range-limited owing to the sparse visibility coverage.

Cores were undetected or could not be unambiguously identified in five cases (SGRSC J0020−7321, J0622−5938, SGRS J0326−7730, J0810−6800 and J1259−7737). We re-observed these five sources in the 6-cm band using the ATCA in the 6A array configuration during 2002 November (see Table 2). These multi-channel continuum observations were made using a pair of 128-MHz bands centred at 4800 and 5952 MHz. Each target was observed for a total of 4 hr with the total time distributed over hour angle as before. Bandwidth synthesis was used to image the visibility data in MIRIAD; the images had beam FWHM in the range 2″–3″. The rms noise in the resulting images was about 0.03 mJy beam^{-1}. Excepting SGRSC J0622−5938, the observations showed compact cores between the diffuse radio components in all the doubtful cases.

In sources of large angular size the region between the lobes where one might expect to find the radio core that is coincident with an optical counterpart is large and, therefore, there might be ambiguities in the identification of the host. In some cases supporting evidence such as connected lobe emission or jet-like features might provide confirmation for the identification. Examining our high resolution ATCA images that were used for detecting radio cores of the giant radio galaxy candidates, we find that there is on the average about 1 compact radio source coincident with an optical galaxy in regions of about 140 square arcmin (avoiding the regions close to the giant radio sources). On the average, the sky area that we searched for optical counterparts of individual giant radio source candidates is about 5 square arcmin. We infer that the probability of occurrence of a random compact object in

the area where we look for IDs is 0.04 and that ambiguities might be expected in only 4% of the cases.

In five sources (SGRSC J0200−6007, J0603−5429, J1959−6402, J2150−6210 and J2253−5813), the angular separation between compact components that were detected at the ends of the extended SUMSS components was less than $5'$ and, therefore, these sources were excluded from further consideration for our giant radio source sample. In SGRSC J0020−7321 and J0129−6433 the ATCA observations revealed a compact component in only one lobe and in SGRSC J2228−5600 no hotspots were seen; the ends of these sources as seen on SUMSS images were $\lesssim 5'$ and they would not be included in the complete sample. However, they were retained for the optical spectroscopy.

The connectedness between the close components in SGRS J0400−8456, SGRSC J0414−6933 and J1920−7753 was not established in the SUMSS images; therefore, we made somewhat higher resolution 20-cm band ATCA observations of these sources in 1.5-km array configurations. The SW component of SGRSC J1920−7753 was observed to have a triple structure and is probably an independent radio source. The northernmost component of SGRSC J0414−6933 appeared to be a separate unresolved source and the remainder a triple of angular size less than $5'$. Therefore, these two sources are rejected by our selection criteria. Two other sources (SGRSC J0622−5938 and J0745−7732) were rejected because an examination of their SUMSS extended structure together with the ATCA compact components suggested that these source structures are peculiar and are very unlike our expectations for double radio sources. The details of these observations are given below in Section 5 and in the Appendix as part of the notes on individual sources.

Composite images made by overlaying ATCA radio contours on SuperCOSMOS sky survey (SSS) greyscales were examined for any optical counterparts. In some cases, the optical images showed galaxies coincident with compact radio components located within each of the close pair of extended radio sources. These were deemed to be separate radio sources created by the separate optical identifications and not related double structures created by twin beams from a single AGN. There were 4 such candidates (SGRSC J0152−8020, J0534−8203, J0551−5655, J2222−5617) that were rejected for this reason.

There were, in all, 22 giant radio source candidates that satisfied the criteria of angular size, declination and latitude.

4. Optical spectroscopy of the host galaxies

The redshifts of six of the 22 giant radio source candidates had been measured previously
(SGRSC J0020−7321, J2336−8151, SGRS J0143−5431, J1919−7959, and J2159−7219 by Boyce (2000); SGRS J0515−8100 by R. Subrahmanyan et al. (2005, in preparation)). The spectra in Boyce (2000) were obtained in service mode at the 3.9-m Anglo-Australian Telescope. The remaining 16 were observed in multiple sessions using the Dual Beam Spectrograph (DBS) on the ANU 2.3-m telescope (Rodgers et al. 1988) to obtain optical spectra for measuring redshifts. A journal of the optical spectroscopy is in Tables 3 and 4.

We were initially allocated a total of 7 nights of dark time. These were in two separate observing runs in 2002 August (4 nights) and 2002 November (3 nights) and 14 objects were observed in these sessions (Table 3). Only the last night in the August session and the later two nights in the November session were without cloud for most of the night and had average seeing of $\approx 1\farcs7$. The other nights were mostly lost due to cloud.

Three of the objects were too faint to give reliable redshifts. Additionally, the identifications of two other sources were revised on the basis of ATCA observations that were scheduled following the optical spectroscopy. We reobserved three of these candidates—SGRS J0810−6800 (new id), J1911−7048 and J1946−8222—along with SGRS J1259−7737 that had not been observed in the earlier sessions, on two additional nights in 2004 April. These nights were clear with average seeing of $1\farcs5$. The two other sources—SGRS J0237−6429 and J0326−7730 (new id)—were observed in a separate run in 2004 September. These later observations are listed in Table 4.

A low resolution grating, 158R lines/mm was used, giving a wavelength coverage of 3600–10900 Å with a spectral resolution of 8 Å ($\sim$ 2 pixels). The red arm of the DBS was used for the observations listed in Table 3 whereas the blue arm was used for the observations listed in Table 4. Most objects were observed in a single 2000-s exposure; however, fainter objects required longer integration times. To calibrate for atmospheric absorption a smooth spectrum star was also observed at roughly the same zenith angle as the target observations. In the 2002 observing runs each target and smooth spectrum standard frame was sandwiched between two short exposures of a Ne-Ar arc for wavelength calibration; a Cu-Ar arc was used in the later runs. A slit width of $2''$ was used for the target observations as well as the arc exposures.

The standard IRAF reduction package was used for the analysis. The raw 2-dimensional spectra were corrected for CCD bias after which they were flat-fielded using averaged dome and sky flats. In extracting the 1-dimensional spectra of the targets the sky background

was averaged over nearby rows on either side of the target trace to minimise effects due to curvature in the spatial axis. The cosmic rays were removed by setting the flux ratio parameter for a given flux threshold using COSMICRAYS; the flux ratio versus threshold plot of the CCD frame was examined for setting the values. This method worked well enough up to a certain flux ratio but beyond that it was nearly impossible to reduce the value further without also affecting the target spectrum adversely. Objects observed in the sessions listed in Table 4 had multiple exposure frames and, after calibration, these were combined using SCOMBINE; the resulting spectra were relatively free of artefacts. The 1-dimensional spectra were divided by the normalised fit to the continuum of a smooth spectrum star to remove atmospheric absorption.

We used the IRAF task RVIDLINES for determining the redshifts. We checked for broad consistency between the redshift and the apparent magnitude of the target. Several objects were independently analysed by two of us, using different software packages, and we obtained identical results: this gives confidence in the redshift estimates.

The redshifts were used to derive the linear sizes of the 22 candidates. Four sources (SGRSC J0020−7321, J0129−6433, J2228−5600 and J2336−8151) had linear size < 0.7 Mpc and were excluded from the giant radio source sample on this basis. We were unable to obtain a reliable spectrum for SGRS J1259−7737 because of the faintness of the optical host; assuming that the faintness implies a high redshift, we have chosen to retain this source in our giant radio source sample (see the notes on this source in Section 5.1).

5. Results

Table 5 presents the final sample of 18 radio sources satisfying the criteria: $|b| > 12.^{\circ}5$, $\delta < -50^{\circ}$, angular size $> 5'$ and linear size larger than 0.7 Mpc; the table lists some observed properties of the sources. In order to estimate the angular sizes of the giant radio sources, we measured the peak-to-peak separation using the higher resolution ATCA images in those cases where hotspots were detected at both ends, and used the SUMSS 843 MHz maps for the remaining sources. Table 6 lists the positions and flux densities of the radio cores in these 18 giant radio sources. The radio sources in the initial list of candidates that were deemed not to be giant radio sources on the basis of the radio-optical follow-up observations are listed separately in the Appendix, along with their observational data.

The composite radio images of all 18 giant radio sources are given in Figs. 1–18; contours of the higher resolution ATCA images are shown using thin lines and the low-resolution SUMSS images are shown using thick contours; these are shown overlaid on grey scale

representations of SSS optical fields.

The optical spectra of the host galaxies of the giant radio sources are shown in Fig. 19. The spectra are not flux calibrated. The reduced spectra often have spurious features as a result of errors in sky subtraction and cosmic rays and we have identified some of these in the panels of Fig. 19. In Table 7 we list the lines identified in the different objects and give the estimated redshifts derived from fits to these lines.

In Table 8 we list some source properties derived from the observations: linear sizes, core powers, the integrated source powers and host absolute magnitudes.

5.1. Notes on individual sources

5.1.1. SGRS J0047−8307 (Fig 1)

In the SUMSS 843 MHz image the source is seen as a triple; there are noticeable gaps in the radio emission between the lobes and the core. The lobe with the smaller separation from the core is also the brighter of the two lobes. The ATCA image shows two compact components in the NW lobe; however, in the southern lobe there is only a weak component close to the peak of the extended emission. The extension seen in the SE lobe at 843 MHz towards NW might be confused with emission associated with a relatively bright, $b_j = 17.8$, elliptical galaxy that is host to a compact $S_{1.4} = 6.4$ mJy source. The host galaxy, which is coincident with the radio core, has a close neighbour 5″ to the south and another 12″ to the west. The optical spectrum has low signal-to-noise ratio; the identification of [OIII]5007 is uncertain because of its proximity to night sky [OI]6300.

5.1.2. SGRS J0143−5431 (Fig 2)

The SUMSS 843-MHz image shows a relaxed morphology for the two lobes and the higher-resolution 1.4-GHz ATCA image shows no compact features associated with the lobes. The ATCA image (Fig. 2b) shows a radio core and, interestingly, this image also shows two compact features on either side of the core and along the source axis: this triple structure at the core together with the relaxed outer lobes suggest the possibility that SGRS J0143-5431 might be a case where an inner double has been created by a restarting of the beams from the central engine. The host galaxy has a few, relatively faint neighbours within 15″ radius and a bright galaxy 30″ to the SE. The close faint neighbour 5″ to the West is a blue object and the galaxy 12″ to the North is a spiral. The optical spectrum of the host galaxy was

obtained by Boyce (2000).

5.1.3. SGRS J0237−6429 (Fig 3)

The SUMSS image shows two lobes with surface brightness decreasing towards the centre and prominent gaps in the emission between the core and the two lobes. The ATCA image shows a weak core and compact features at the ends of both lobes. The closer lobe is also the brighter of the two lobes. The host galaxy does not have any close neighbours. The optical spectrum is very noisy and the redshift is uncertain.

5.1.4. SGRS J0326−7730 (Fig 4)

This source has an unusual structure. The SUMSS image shows two extended components of which the SE is significantly stronger. The higher resolution 1.4-GHz ATCA image reveals a bright elongated structure in this SE lobe. Although edge-brightened, there is no compact unresolved feature towards the outer end of this lobe. The ATCA image also shows a compact component at the peak of the NW lobe. The 4.8-GHz ATCA image (Fig. 4b) shows a weak core coincident with a faint galaxy that is located within the SUMSS contours of the stronger lobe and close to the line joining the compact features in the two lobes. The host galaxy has several faint galaxies in its neighbourhood.

5.1.5. SGRS J0331−7710 (Fig 5)

This radio source has the largest linear size in the sample and is extremely asymmetric in lobe separation as well as lobe brightness and flux density. Both lobes are highly elongated with high axial ratios and both elongated lobes are collinear. The two lobes are edge brightened; however, the contrast in surface brightness along the lobe axes is relatively weak in this source. In the ATCA image the two lobes are completely resolved and a weak core is detected at the inner end of the northern lobe (Fig. 5b); there is a significant emission gap of almost 600 kpc between the core and the southern lobe. The host galaxy is fairly isolated except for a close neighbour $\sim 10''$ to the SW. There is a prominent halo associated with the host galaxy that appears asymmetric in the blue image, with an extension to the north.

5.1.6. SGRS J0400−8456 (Fig 6)

The SUMSS image shows several emission peaks that are not all collinear. The ATCA image shows a central source coincident with a galaxy; this radio core has twin jets on either side (Fig. 6b). The SUMSS peaks to the north and south of the central component have compact features in the ATCA images. In the SUMSS image there is an extension from the northern peak towards west that is oriented nearly orthogonal to the inner radio axis. There is a similar bend in the southern lobe towards SE. Compact structure is seen associated with the southernmost component in the high resolution ATCA image. There is no optical identification at this location. We are not certain if this component is a part of the giant radio galaxy and do not include it in the size determination. A low-resolution 1.4-GHz ATCA image made using the 1.5 km array is shown Fig. 6(c); the connectedness of the differrent components of the source is seen more clearly in this image. We have conservatively estimated the angular size to be the sky angle between the outer components of the source in Fig. 6(c). The source is edge-darkened, it is also one of the lowest power sources in the sample and the source may be classified as FR-I type. The multiple peaks on either side of the core have Z-symmetry: this is suggestive of multiple activity episodes in a precessing jet. The host is a relatively bright $b_j = 16.9$ galaxy with several close neighbours within $1'$ radius.

5.1.7. SGRS J0515−8100 (Fig 7)

This double radio source has extremely low surface brightness lobes that have an extremely low axial ratio; the higher resolution ATCA observations have detected a faint radio core coincident with a galaxy that is located at the inner end of the southern lobe (Fig. 7b). There is an emission gap between the core and the northern lobe. This source appears to be a giant fat double radio source and is being studied in detail by R. Subrahmanyan et al. (2005, in preparation). The optical spectrum of the host galaxy was obtained by Vincent McIntyre and Carole Jackson in 1999 using the DBS at the SSO 2.3-m telescope.

5.1.8. SGRS J0631−5405 (Fig 8)

This giant radio source is a quasar. The SUMSS image shows a pair of lobes; the higher resolution ATCA image shows a strong radio core coincident with a star-like object. The ATCA image shows compact structure at the end of the western lobe whereas the eastern lobe appears resolved. The western lobe has a smaller extent from the core and also has a

higher surface brightness. There is an emission gap between the core and the lower-surface-brightness eastern lobe. The quasar has been catalogued in the Deep X-ray Radio Blazar Survey (Perlman et al. 1998) and is a known X-ray source in the ROSAT PSPC database of point sources.

5.1.9. SGRS J0746−5702 (Fig 9)

In the SUMSS this radio source appears as a bright extended central source flanked by much fainter lobes. In the higher resolution ATCA image the central source is resolved into a strong core and a jet-like feature to the SW. Both lobes are resolved in the ATCA observations and no compact structure is observed. The jet appears directed towards the fainter of the two lobes. The radio structure at 843 MHz can be classified as FR-I type given the edge-darkened lobes; however, the detection of a one-sided partial jet some distance from the core is unusual and indicates that this source might be another example of a restarting jet within relict lobes. There is a neighboring galaxy situated $\sim 4''$ from the host galaxy in a position angle perpendicular to the radio axis of the source.

5.1.10. SGRS J0810−6800 (Fig 10)

The SUMSS image shows two lobes; the NW lobe is edge-brightened and has the higher surface brightness. A compact source is detected at the peak of the NW lobe in the ATCA 1.4-GHz image; the SE lobe is completely resolved. The ATCA image at 4.8 GHz (Fig. 10b) revealed a faint radio core coincident with a star-like object that is located on the line joining the outer ends of the two lobes. The lobes do not, however, extend along this line and appear directed to the north of the axis in both cases. The host object has very broad Hβ and Hα emission lines and is a quasar. The host object is star-like in blue; however, in the red SSS images it is surrounded by three faint patches of emission. An unusual aspect of this giant radio source is that although it has a broad-line host, the radio core is weak. An unusual feature of the spectrum is the associated blue-shifted absorption in the Balmer lines, indicating the presence of recent star formation.

5.1.11. SGRS J0843−7007 (Fig 11)

The radio structure of this giant radio source resembles SGRS J0746−5702 in that it has a central, bright component straddled by two extended lobes with low surface brightness. In

the higher resolution ATCA image only a central radio core is detected; the two low-surface-brightness lobes are completely resolved. The host galaxy has a close neighbour $\sim 10''$ to the north. This source might be a relic of a giant FR-II radio source in which the beams from the central engine no longer energize the lobes.

5.1.12. SGRS J1259−7737 (Fig 12)

This giant radio source has prominent lobes and is clearly seen to be an edge-brightened double radio source. The two lobes extend all the way towards each other without any emission gap. The 1.4-GHz ATCA high-resolution image detected compact hotspots at the ends of both lobes and later 4.8-GHz ATCA imaging detected an additional weak compact core close to the centre of the radio source (Fig. 12b). The core is coincident with a faint object at the plate limit. The sky region in which the host galaxy lies appears relatively devoid of optical objects suggesting dust obscuration along this line of sight. In spite of 5×2000 s exposure on the 2.3-m telescope we were unable to obtain a firm redshift for this galaxy because of its faintness. A K-band image of the field was obtained for us by Helen Johnston with the Cryogenic Array Spectrometer/Imager (CASPIR) on the ANU 2.3-m telescope at Siding Spring Observatory. A host galaxy is clearly detected at the location of the radio core. We estimate its K magnitude to be 16.2 $\pm$0.2; using the K-z relation for radio galaxies we estimate its redshift to be > 0.3. Its linear size is estimated to be > 1.5 Mpc.

5.1.13. SGRS J1336−8019 (Fig 13)

In the SUMSS this double radio source appears to have an edge-brightened structure with a high axial ratio. The higher resolution ATCA image shows a chain of weak compact features that trace the chain of peaks observed in SUMSS indicating the presence of a weak two-sided jet along the central line of this radio source. The strongest among the emission peaks is the central core component and this coincides with the southern member of a close pair of objects (Fig. 13b) which were partly blended on the spectrograph slit. The presence of Hα absorption in the host galaxy spectrum indicates that the northern object is a star. The ATCA image also detects a feature at the leading edge of the southern lobe; however, there is no recognizable equivalent feature at the leading edge of the northern lobe.

5.1.14. SGRS J1728−7237 (Fig 14)

The source is a triple in both the SUMSS and ATCA images. There are large emission gaps between the lobes and the core. This is an asymmetric source with the northern lobe closer to the core as compared to the southern lobe. The ATCA image detects a radio core that is displaced $\sim 7''$ from a bright star and coincident with a faint galaxy, which has a prominent narrow emission-line spectrum. There are several faint galaxies visible in the neighbourhood of the host.

5.1.15. SGRS J1911−7048 (Fig 15)

The large-scale radio structure indicates a low-surface-brightness edge-brightened radio source with a continuous bridge connecting the two lobes. In the higher resolution ATCA image only a core is detected at the centre of the source and coincident with a faint galaxy; the rest of the lobe structure is completely resolved.

5.1.16. SGRS J1919−7959 (Fig 16)

This giant radio source was observed earlier by Subrahmanyan et al. (1996). The SUMSS image shows a pair of prominent lobes; the ATCA image detects structure in both these lobes. Additionally, the ATCA image from Subrahmanyan et al. (1996) detects a weak core between the two lobes and coincident with a faint $b_j = 22.7$ galaxy. Inspection of the digitized plates reveals significant dust obscuration. The optical spectrum was obtained by RWH in 1994 using the Faint Object Red Spectrograph on the Anglo-Australian Telescope.

5.1.17. SGRS J1946−8222 (Fig 17)

The high resolution ATCA image of this source shows a compact, weak core component coincident with a faint host galaxy; the core is straddled by a pair of partial jet-like features that are symmetrically located on either side of the core. The SUMSS image shows extended emission around this central structure as two lobes that have a high axial ratio. The two ends of the source are asymmetrically located with respect to the core. There are no prominent compact hotspots seen at the ends of the source in the 1.4-GHz ATCA image. The inner partial jets might be a case of restarting beams in this giant radio source. The host galaxy is barely seen in the blue, while in the red the host appears as a point-like feature with faint

extended optical emission. We twice attempted to obtain a redshift for this galaxy but poor observing conditions allowed only a tentative estimate.

5.1.18. SGRS J2159−7219 (Fig 18)

In the SUMSS this source has an edge-brightened outer structure and a central triple structure with emission gaps between all components. There is a larger emission gap between the northern lobe and the core. In the ATCA 1.4-GHz image a compact radio core is detected at the location of the central component and this coincides with a bright galaxy (Fig. 18b). At this higher frequency and resolution the only other structure seen is the stronger southern component of the central triple. The host galaxy has a prominent halo; fainter companions are seen in its neighbourhood and the host is likely to be in a cluster environment. The optical spectrum was obtained by Boyce (2000).

6. Discussion

SUMSS has an rms noise of about 1 mJy beam^{-1} and a 5σ surface brightness detection limit of about 12 mJy arcmin^{-2}. With a beam that has a FWHM close to $1'$, it is the best survey today for finding low redshift giant radio sources in the southern sky. The sample of giant radio sources that we have compiled from SUMSS and presented in this paper is the only complete sample in the south.

We find 18 giant radio sources in the 2100 square degrees of search area. There are 4 giant radio sources in this sample with redshifts $z \leq 0.13$: these are in the comoving search volume of 3.5×10^7 Mpc^3 for which the survey is expected to detect all edge-brightened giant radio sources with projected linear size exceeding 0.7 Mpc. This implies that the space density of giant radio galaxies is about 10^{-7} Mpc^{-3} at the survey sensitivity or that a giant radio source is expected per (215 Mpc)^3 in the local universe.

The space density of powerful FR-II radio sources in the local universe is about 10^{-7} Mpc^{-3} (Padovani & Urry 1992). Of the four giant radio sources we detect at $z \leq 0.13$, SGRS J0400−8456 is a FR-I radio galaxy while the remaining three (SGRS J0515−8100, J0746−5702 & J2159−7219) are sources with relaxed—possibly relic—lobes and have radio luminosities significantly below the FR-I/FR-II break luminosity of 1.3×10^{25} W Hz^{-1}. None of the giant radio galaxies in our sample at $z \leq 0.13$ is a classic powerful radio source: none of them has hotspots within the lobes and none of them is above the FR-I/FR-II break in radio luminosity. Within the comoving search volume of 3.5×10^7 Mpc^3 where the survey is expected to detect all edge-

brightened giant radio sources with projected linear size exceeding 0.7 Mpc, all the giants we detect have relict lobes suggesting that *at low redshifts giant radio sources with relict lobes are more numerous than active giants in which the lobes are energized by beams from the centre.* The lack of powerful edge-brightened giant radio sources in this survey volume is consistent with the expected small number of powerful edge-brightened radio sources given the small search region. It is likely that the giant radio sources we detect at $z \leq 0.13$—which have edge-brightened relict lobes—are relics of FR-II giant radio sources. The characteristics of these $z \leq 0.13$ sources allow us to make the tentative inference that FR-II giant radio sources may have much shorter lifetimes in the active phase as compared to the time for which their fading relict lobes remain visible above the survey sensitivity limit.

46 giant radio sources were found in the WENSS survey area of 8100 square degrees north of declination $\delta = +28^\circ$ (Schoenmakers et al. 2001). The angular size and linear-size cutoffs in the selection of WENSS giants was the same as the criteria we have adopted here. The WENSS sensitivity varied with declination: assuming that giant radio sources have a spectral index $\alpha = -0.7$–-1.0 ($S_\nu \propto \nu^\alpha$), the WENSS has a sensitivity to these extended sources that is somewhat better than the SUMSS sensitivity in the sky north of $\delta = +74^\circ$ and comparable in most of the survey region $+28^\circ < \delta < +74^\circ$. In the 600 square degrees where the surface brightness sensitivity in the WENSS is better, the detection rate in the WENSS search is a factor 1.7 higher. However, in the 7500 square degrees where the surface brightness sensitivity of the WENSS is comparable to that of the SUMSS, the detection rate in the WENSS is only 0.6 of that in our SUMSS based search. It may be noted that Lara et al. (2001) have pointed out that as many as 8 giant sources at $\delta > +60^\circ$ were missed being selected in the compilation of Schoenmakers et al. (2001).

Barring two giant radio sources (SGRS J0400−8456 and J2159−7219) none of the SUMSS giant radio sources in the sample presented here are likely to belong to clusters. We examined their galaxy environments in the SSS fields and we find them to be isolated, having close companions or in a small group of galaxies.

Six of the eighteen giant radio sources in the sample show classic FR-II radio morphology with compact hotspots at each of the lobe ends (SGRS J0047−8307, J0237−6429, J0631−5405, J1259−7737, J1728−7237 and J1919−7959). SGRS J0810−6800 and J1336−8019 are FR-IIs with compact structure at the end of only one lobe; in both these sources the ATCA images show no compact component in the other lobe.

SGRS J0326−7730 and J0331−7710 have large scale SUMSS structures that are highly asymmetric in lobe flux density and lobe separation from their cores. Of these, SGRS J0326−7730 is observed to have structure at the end of one lobe in the ATCA image; SGRS J0331−7710 is not observed to have any compact structure in either lobe.

Seven sources show relaxed lobes with no compact hotspots at either end (SGRS J0143−5431, J0515−8100, J0746−5702, J0843−7007, J1911−7048, J1946−8222 and J2159−7219). All these seven sources with relaxed lobes are among the relatively low-radio-power sources in the sample; this is consistent with the interpretation that these are relic sources in which beams do not currently feed the outer relaxed lobes. Of these, SGRS J0143−5431, J0746−5702, J1946−8222 and J2159−7219 have evidence for either one or two sided knots/jets closer to the nucleus and might be examples of giant radio sources with relict lobes and restarting beams.

SGRS J0400−8456 is the only source in the sample that is observed to have highly-bent tail-like lobe structures that decrease in surface brightness away from the centre. This source appears to have a pair of jets close to the centre and might be a giant edge-darkened radio source. The source has among the lowest radio powers in the sample and this is consistent with the FR-I type structure.

The SUMSS is a survey with high surface brightness sensitivity; nevertheless, a large fraction (11/18) of the giant radio sources in the sample are observed to have emission gaps between the lobes. Continuous bridges are observed in SGRS J0400−8456 J0746−5702, J0843−7007, J1259−7737, J1336−8019, J1911−7048 and J1919−7959.

There are two quasars in the sample. Both the quasars (SGRS J0631−5405 and J0810−6800) have prominent lobes and have significantly more compact emission detected at the end of one of their lobes. While J0631−5405 has a bright radio core consistent with it being a quasar, the core in J0810−6800 is relatively weak. In both quasars the brighter lobe is observed to be closer to the core and is also the one containing the hotspot. No jets are seen in the ATCA images associated with the cores in these sources. Compared to the sources in the sample with classic FR-II structure that have hotspots at one or both ends of the lobes, the two quasars have wider lobes with significantly lower axial ratio. It may be noted here that if the quasars are significantly fore-shortened owing to projection, their linear sizes might be significantly larger than the estimates given in Table 8 and, therefore, these quasars are potentially the sources with the largest linear size in the sample. The giant quasars have intermediate radio powers compared to other giant radio sources in our sample.

The quasar fraction that we detect (two quasars in the sample of 18 giant radio sources) is smaller than that expected on the basis of the unification model for radio galaxies and quasars (Barthel 1989). This might be because giant radio sources with larger linear sizes are relatively rarer and our lower limit of $5'$ to the angular size of sources accepted into the sample might imply a larger linear-size cutoff for quasars as compared to radio galaxies.

Seven of the host galaxies of the giant radio sources in the sample have detections of narrow emission lines. Of these SGRS J0326−7730, J1728−7237 and J1919−7959 have relatively stronger emission lines whereas the emission lines in SGRS J0047−8307, J0237−6429, J0515−8100 and J1336−8019 are weaker. The giant radio sources in the sample with relatively higher redshifts and radio powers appear to be the ones with emission lines in their host spectra.

Asymmetry in lobe extents appears to be a characteristic of the sample. We define an asymmetry parameter as the ratio of the separation from the core of the farther lobe to the separation from the core of the closer lobe; distances to both lobes are measured to their farthest emission peaks. If we exclude the two quasars that might be affected by projection because their axes are likely to be at relatively smaller angles to the line of sight, 11 of the 16 giant radio sources have asymmetry parameter $\gtrsim 1.25$: nearly 70% of the sample has radio lobes that are longer on one side by $\gtrsim 25\%$. Among the most asymmetric is SGRS J0331−7710 in which the southern lobe extends to $\gtrsim 2.5$ times the distance of the northern lobe from the core.

Of the 11 asymmetric giant radio sources, the closer lobe is also the brighter of the two lobes in as many as 10 cases. This statistically significant result, which was earlier noted by Saripalli et al. (1986) for a small set of giant radio sources, has also been seen in other samples of giant radio sources (Schoenmakers et al. 2000b; Lara et al. 2001; Machalski et al. 2001). We do not, however, find a correlation between the lobe separation asymmetry and the lobe brightness asymmetry: although SGRS J0331−7710 is the most asymmetric in lobe separation and has lobes that are also very asymmetric in brightness it is not among the most asymmetric in lobe brightness in the sample.

We define the misalignment angle as the supplement of the angle subtended by the two outermost hotspots at the core. Excluding the two quasars, the bent FR-I SGRS J0400−8456 and the sources that have lobes with small axial ratio and no compact structure (SGRS J0143−5431, J0515−8100, J0746−5702 and J0843−7007), the distribution of misalignment angles shows that all the remaining 11 sources are aligned to within 10° over the megaparsec distance; 7 of the 11 are aligned to within 5°.

The median linear size of our SUMSS sample is 1.3 Mpc and the median total power is 5×10^{25} W Hz^{-1}. The giant radio sources in the sample have luminosities spread over more than two orders of magnitude covering the range $10^{24} < P^{843}_{total} < 5 \times 10^{26}$ W Hz^{-1}, straddling the FR-I/FR-II break. The SUMSS giant radio sources exhibit increasing core power with total power: the correlation coefficient between the logarithm of the core power at 1.4 GHz and the logarithm of the total power at 843 MHz is only 0.5 for our sample; however, the fit is consistent with that found by Giovannini et al. (2001) for B2 and 3CR

radio galaxies that cover a larger range in total luminosity but having smaller linear size. In spite of its relatively low total power, SGRS J0746−5702, which has a prominent partial jet towards its SW lobe, has a core power that is well above this fit to the core power versus total power: this is consistent with the the earlier hypothesis that SGRS J0746−5702 is a restarted source. The only giant radio source in the sample with strong, narrow emission lines (SGRS J1728−7237) also has the most powerful radio core. Surprisingly, the giant radio source in our sample with the lowest core power is a quasar (SGRS J0810−6800).

7. Summary

We have presented a complete sample of 18 giant radio sources compiled from the SUMSS; the sample satisfies the selection criteria: Galactic latitude $|b| > 12.^{\circ}5$, declination $\delta < -50^{\circ}$ and angular size $> 5'$. All the sources have projected linear size larger than 0.7 Mpc (assuming $H_o = 71$ km sec^{-1} Mpc^{-1}). Higher resolution ATCA radio observations at 1.4 GHz have been used to identify radio cores and hotspots and distinguish any unrelated radio sources in the original candidate list. This facilitated optical identification and subsequent optical spectroscopy using the DBS at the 2.3 m SSO telescope and resulted in near complete redshift information for our sample. The redshift range of the sample is 0.09−0.48. The 18 giant radio sources have powers straddling the FR-I/FR-II break power.

The SUMSS giants have radio morphologies that are mostly edge-brightened although several have lobes with no compact features in them. Asymmetric lobe separation from their cores is widely seen and a significant correlation exists between lobe separation and lobe brightness: the closer lobe is nearly always the brighter.

We detect all giants with linear size larger than 0.7 Mpc in the nearby universe ($z \leq 0.13$). However, given the selection criteria, there is inherently a redshift-dependent linear-size bias at higher redshifts. Within this survey area ($z \leq 0.13$), not one of the four giants we detect has edge-brightened structure with compact hotspots. All four giants have among the lowest powers in the sample and three have lobes with relaxed morphologies. If the three with relaxed morphologies are relicts of FR-II giants this suggests that in the nearby universe there could be an overabundance of giant radio sources with relict lobes as compared to giants whose lobe ends are currently energized by beams.

The SUMSS sample has several interesting sources. The sample contains one of the most asymmetric giant radio sources SGRS J0331−7710 where not only is one lobe about 2.5 times closer to the core than the opposite lobe, it is also more than 2.5 times brighter. The four giant radio sources: SGRS J0143−5431, J0746−5702, J1946−8222, J2159−7219

as well as SGRSC 0414−6933 are candidates for re-started activity: all have relaxed outer lobes and either a pair of inner lobes that might be a manifestation of new beams from the central engine or partial jets close to the centre.

The MOST is operated by the University of Sydney and supported in part by grants from the Australian Research Council. The Australia Telescope Compact Array is part of the Australia Telescope which is funded by the Commonwealth of Australia for operation as a National Facility managed by CSIRO. We acknowledge the use of SuperCOSMOS, an advanced photographic plate digitizing machine at the Royal Observatory of Edinburgh, in the use of digitized images for the radio-optical overlays. We thank Anton Koekemoer for discussions in the early part of the project and for advice on some IRAF tasks. We thank Helen Johnston for the K-band image of SGRS J1259−7737.

A. CANDIDATES NOT IN THE COMPLETE SAMPLE OF GIANT RADIO SOURCES

In Figs. 20–28 we present 843 MHz SUMSS and higher resolution ATCA images of a selection of giant radio source candidates from the original list that did not satisfy one or both criteria: angular size $> 5'$ and projected linear size larger than 0.7 Mpc. We obtained low-resolution optical spectra using the DBS on the 2.3-m SSO telescope for the host galaxies of some of these candidates and Boyce (2000) obtained AAT spectra for some hosts; the spectra are presented in Fig. 29. Table A1 lists the prominent spectral lines and the derived redshifts. In Table A2 we give the sizes and structural type for some of these radio sources. In Table A3 we list their radio core positions and the 1.4-GHz core flux densities. For all the sources from the original giant radio source candidate list that were rejected from the final sample we give below brief notes.

A.1. SGRSC J0020−7321 (Fig 20)

The SUMSS image shows a filled radio structure over its $4\farcm8$ extent. In the higher resolution 1.4-GHz ATCA image the eastern lobe is completely resolved (Fig. 20a). There is structure seen in the western lobe; however, no compact hotspot is observed. The 4.8-GHz ATCA image detects a core at the position of a bright galaxy (Fig. 20b). Twin-jet like structures are seen at the core and aligned with the source axis; the western jet appears to curve towards the bright elongated structure in the western lobe. The host has a close companion $4''$ to the NW and there is a prominent halo surrounding the galaxy pair. This candidate is rejected because it fails the angular-size criterion. The optical spectrum was obtained by Boyce (2000).

A.2. SGRSC J0129−6433 (Fig 21)

The SUMSS image shows a filled radio structure with a straight edge along its SW boundary. The radio structure is reminiscent of the structure seen in 3C430 and 3C111 where one edge of the radio galaxy has a straight edge and lobe emission on the opposite side extends away perpendicular to the radio axis. The ATCA image shows a compact feature that appears to be a multiple hotspot structure at the end of the SE lobe; the northern lobe is resolved. There are two presumably unrelated sources seen in the ATCA image within the southern lobe. The host galaxy of this source has strong narrow emission lines and is fairly isolated. The closest neighbours are about an arcminute away to the SE and SW. The

candidate fails the angular-size criterion and is excluded from our sample.

A.3. SGRSC J0152−8020

In the SUMSS image (not shown) the source is seen as two extended components separated by about 5.′5. Both components of this candidate are detected in the higher resolution ATCA observations in which the SW source is identified with a faint optical object and the NE source has a double structure in position angle −20°. The candidate is rejected because the western component is identified and both SUMSS components are likely to be separate sources.

A.4. SGRSC J0200−6007 (Fig 22)

Two prominent lobes are observed in the SUMSS image. The ATCA observations detect structure in both lobes; additionally, a compact core is detected between the two components. The core is identified with a faint $b_j = 21.2$ galaxy; we have not obtained an optical spectrum for the host galaxy. This candidate is rejected because its angular extent is less than 5′.

A.5. SGRSC J0414−6933 (Fig 23)

Four extended components are seen in the SUMSS image of this candidate. Higher resolution ATCA image shows a compact source coincident with the Northern-most component. The other three SUMSS components are observed to constitute a separate triple radio source in the low-resolution ATCA image (Fig. 23b): the central component of this triple is resolved into a 45″ triple in the higher-resolution ATCA image (Fig. 23a) and the core is identified with a $b_j = 19.5$ galaxy. The lack of compact features in the two lobes and the central triple structure suggest restarting activity in this radio galaxy. The optical host has a halo that is more prominent in the red and has a sharp edge towards the SW. It has no immediate neighbours although it might be the member of a loose group. The 4.′5 triple radio source is a giant radio source; however, J0414−6933 is not a part of the sample because its angular size is less than 5′. The optical spectrum for this source (Fig. 29) was obtained using the Dual Beam Spectrograph at the 2.3-m telescope at Siding Spring Observatory. The spectrum was obtained from a single 2000-s exposure on 2002 Nov 04.

A.6. SGRSC J0534−8203

This source is observed to be two separate components in the SUMSS image (not shown); the candidate has a total angular size less than 5′ and therefore fails the selection criterion. In the ATCA image (not shown) the eastern component is resolved into a 1′ triple; there is a faint blue galaxy very close to the central component of this triple, which is likely to be the host galaxy for the eastern SUMSS component. The western component is resolved into three compact sources none of which has an optical counterpart in SSS.

A.7. SGRSC J0551−5655

This source consists of three extended components in the SUMSS image (not shown). Higher resolution ATCA observations show the western component to be a double centered on an optical galaxy; additionally, compact components without optical counterparts in SSS images are detected coincident with the other two SUMSS components. The candidate has an angular size less than 5′ and hence fails the selection criteria.

A.8. SGRSC J0603−5429

In the SUMSS image (not shown) the source is seen as three peaks that are connected by extended emission. In the higher resolution 1.4-GHz ATCA observations the SE peak appears as an unresolved component without any optical counterpart in SSS images. The remaining two peaks are also detected: they are weaker and appear to be coincident with two faint galaxies. This source is rejected as a candidate because its peak-to-peak angular size is less than 5′.

A.9. SGRSC J0622−5938

In the SUMSS image (not shown) the source appears as two components that are extended roughly towards each other with a faint bridge of emission connecting them. The ATCA detects weak components at the two peaks and these have no optical counterparts in SSS images. The candidate has an angular size less than 5′ and fails the selection criteria.

A.10. SGRSC J0745−7732

In both the SUMSS and the ATCA images (not shown) this source is observed to be a chain of nine unresolved radio sources arrayed along a position angle of about 45°. Some of the components are extended along this position angle in the SUMSS; however, there is no diffuse emission connecting these individual sources. Only two components have faint objects associated with them in the blue SSS image. Apart from being in a line, there is no evidence from either the SUMSS or ATCA observations that the remaining components form a single source and, therefore, we do not accept this into our giant radio source sample.

A.11. SGRSC J1920−7753 (Fig 24)

The SUMSS image shows a very elongated radio structure directed towards a component to the NE (Fig. 24a). Low-resolution 20-cm ATCA imaging revealed that the elongated source is a triple (Fig. 24b). In the higher resolution ATCA image the elongated source is resolved into a series of peaks and the brightest (with flux density 19.4 mJy beam^{-1}) is identified with a very faint object that is seen only in the red SSS image. The NE component is detected as an unresolved source without any optical ID in SSS. Because the SUMSS components are deemed to be separate sources that are $< 5'$ in size, the source is excluded from the sample.

A.12. SGRSC J1959−6402 (Fig 25)

The SUMSS image shows this source to be two edge-brightened lobes; ATCA images show compact hotspots at the leading edges. A weak core is detected with a flux density of 4.3 mJy beam^{-1} at 1.4 GHz. The angular size as measured between the hotspots detected in the ATCA image is just under $5'$ and the source fails the selection criteria for our sample.

A.13. SGRSC J2150−6210

In the SUMSS image (not shown) the source has a double structure, with significantly different flux densities, and a connecting bridge. The ATCA detects a compact source at the location of the stronger NE component and a weaker source at the peak of the SW SUMSS component. The NE source is identified with a bright elliptical galaxy and is likely to be a separate source. The candidate is rejected as it fails the angular-size criterion.

A.14. SGRSC J2222−5617

Two separate components appear in the SUMSS image (not shown) and the southern component has a weak extension towards the other component. The ATCA observations reveal the two components to be separately a double and a triple. The southern triple is identified in SSS with an elliptical galaxy. The two SUMSS components are likely to be two unrelated radio sources.

A.15. SGRSC J2228−5600 (Fig 26)

The SUMSS image shows this source to be an edge-brightened radio source with a relatively strong core. The 1.4-GHz ATCA image shows only the core component as a strong unresolved source coincident with a relatively bright $b_j = 17.7$ elliptical galaxy. The host is likely to be in a cluster. The galaxy optical spectrum shows the presence of moderately strong emission lines. This source has a linear size of 428 kpc and is not a giant radio source.

A.16. SGRSC J2253−5813 (Fig 27)

The SUMSS image shows an edge-brightened double radio source with a continuous bridge. Higher resolution ATCA observations detect hotspot components at both ends as well as a radio core that is identified with a $b_j = 18.5$ elliptical galaxy. We have not obtained an optical spectrum for this galaxy. This source is not in the sample because its angular size $< 5'$.

A.17. SGRSC J2336−8151 (Fig 28)

The SUMSS image shows a chain of connected components. Our higher resolution ATCA image shows emission features associated with all except the diffuse component at the SE end of the source. A radio core, coincident with an optical counterpart, is detected in an inner component and there is an indication for twin-jet structure close to the core. The radio structure is very asymmetric. This source fails the linear-size criterion and hence is not part of our giant radio source sample. The optical spectrum was obtained by Boyce (2000).

REFERENCES

Barthel, P. D., 1989, ApJ, 336, 606

Becker, R. H., White, R. L., Helfand, D. J., 1995, ApJ, 450, 559

Bock, D. C. -J., Large, M. I., Sadler, E. M., 1999, AJ, 117, 1578

Boyce, E., 2000, Honours Thesis, School of Physics, University of Sydney, http://www.astrop.physics.usyd.edu.au/SUMSS/

Condon, J. J., Cotton, W. D., Greisen, E. W., Yin, Q. F., Perley, R. A., Taylor, G. B., Broderick, J. J., 1998, AJ, 115, 1693

Cotter, G., Rawlings, S., Saunders, R., 1996, MNRAS, 281, 1081

Giovannini, G., Cotton, W. D., Feretti, L., Lara, L., Venturi, T., 2001, ApJ, 552, 508

Lara L., Cotton W. D., Feretti L., Giovannini G., Marcaide J. M., Marquez I., Venturi T., 2001, A&A, 370, 409

Machalski J., Jamrozy M., Zola S., 2001, A&A, 371, 445

Mauch, T., Murphy, T., Buttery, H. J., Curran, J., Hunstead, R. W., Piestrzynski, B., Robertson, J. G., Sadler, E. M., 2003, MNRAS, 342, 1117

Owen, F. N., Ledlow, M. J., 1994, in ASP Conf. Ser. 54, The First Stromlo Symposium: The Physics of Active Galaxies, ed. G. V. Bicknell, M. A. Dopita & P. J. Quinn (San Francisco: ASP), 319

Padovani, P., Urry, C. M., 1992, ApJ, 387, 449

Perlman, E. S., Padovani, P., Giommi, P., Sambruna, R., Jones, L. R., Tzioumis, A., Reynolds, J., 1998, AJ, 115, 1253

Rengelink, R. B., Tang, Y., de Bruyn, A. G., Miley, G. K., Bremer, M. N., Roettgering, H. J. A., Bremer, M. A. R., 1997, A&AS, 124, 259

Rodgers A. W., Conroy P., Bloxham G., PASP, 100, 626

Saripalli L., Gopal-Krishna, Reich W., Kuehr H., 1986, A&A, 222, 300

Saripalli, L., Subrahmanyan, R., Udaya Shankar, N., 2002, ApJ, 565, 256

Saripalli, L., Subrahmanyan, R., Udaya Shankar, N., 2003, ApJ, 590, 181

Schoenmakers A. P., de Bruyn, A. G., Roettgering, H. J. A., van der Laan, H., Kaiser, C. R., 2000a, MNRAS, 315, 371

Schoenmakers A. P., Mack K.-H., de Bruyn A. G., Roettgering H. J. A., Klein U., van der Laan H., 2000b, A&AS, 146, 293

Schoenmakers A. P., de Bruyn, A. G., Roettgering, H. J. A., van der Laan, H., 2001, A&A, 374, 861

Subrahmanyan R., Saripalli L., 1993, MNRAS, 260, 908

Subrahmanyan R., Saripalli, L., Hunstead, R. W., 1996, MNRAS, 279, 257

Willis A. G, Strom R. G., Bridle A. H., Fomalont E. B., 1981, A&A, 95, 250

Table 1. Journal of ATCA observations-1.4 GHz

Name	Array	Date	Time (min)
SGRSC J0020−7321	6D	2001 Nov 26	28
	6A	2001 Dec 14	24
SGRS J0047−8307	6D	2001 Nov 26	28
	6A	2001 Dec 14	24
SGRSC J0129−6433	6D	2001 Nov 25	24
	6A	2001 Dec 14	24
SGRS J0143−5431	6D	2001 Nov 26	21
	6A	2001 Dec 14	24
SGRSC J0152−8020	6D	2001 Nov 25	28
	6A	2001 Dec 14	24
SGRSC J0200−6007	6D	2001 Nov 25	33
	6A	2001 Dec 14	24
SGRS J0237−6429	6D	2001 Nov 25	28
	6A	2001 Dec 14	24
SGRS J0326−7730	6D	2001 Nov 25	35
	6A	2001 Dec 14	24
SGRS J0331−7710	6D	2001 Nov 25	33
	6A	2001 Dec 14	24
SGRS J0400−8456	6D	2001 Nov 25	28
	6A	2001 Dec 14	24
	1.5A	2004 Mar 21	375
	1.5A	2004 Mar 30	310
SGRSC J0414−6933	6D	2001 Nov 25	35
	6A	2001 Dec 14	24
	1.5A	2004 Mar 30	260
SGRS J0515−8100	6D	2001 Nov 25	35
	6A	2001 Dec 14	24
SGRSC J0534−8203	6D	2001 Nov 25	35
	6A	2001 Dec 14	24
SGRSC J0551−5655	6D	2001 Nov 25	35
	6A	2001 Dec 14	24
SGRSC J0603−5429	6D	2001 Nov 25	28
	6A	2001 Dec 14	24

Table 1—Continued

SGRSC J0622−5938	6D	2001 Nov 25	28
	6A	2001 Dec 14	24
SGRS J0631−5405	6D	2001 Nov 25	28
	6A	2001 Dec 14	24
SGRSC J0745−7732	6D	2001 Nov 25	38
	6A	2001 Dec 14	36
SGRS J0746−5702	6D	2001 Nov 25	35
	6A	2001 Dec 14	36
SGRS J0810−6800	6D	2001 Nov 25	35
	6A	2001 Dec 14	30
SGRS J0843−7007	6D	2001 Nov 25	35
	6A	2001 Dec 14	30
SGRS J1259−7737	6D	2001 Nov 25	35
	6A	2001 Dec 14	36
SGRS J1336−8019	6D	2001 Nov 25	35
	6A	2001 Dec 14	36
SGRS J1728−7237	6D	2001 Nov 25	42
	6A	2001 Dec 14	36
SGRS J1911−7048	6D	2001 Nov 25	35
	6A	2001 Dec 14	30
SGRS J1919−7959	6D	2001 Nov 26	28
	6A	2001 Dec 14	24
SGRSC J1920−7753	6D	2001 Nov 26	21
	6A	2001 Dec 14	24
	1.5A	2004 Apr 04	312
SGRS J1946−8222	6D	2001 Nov 26	21
	6A	2001 Dec 14	24
SGRSC J1959−6402	6D	2001 Nov 26	21
	6A	2001 Dec 14	25
SGRSC J2150−6210	6D	2001 Nov 26	28
	6A	2001 Dec 14	24
SGRS J2159−7219	6D	2001 Nov 26	28
	6A	2001 Dec 14	24
SGRSC J2222−5617	6D	2001 Nov 26	21

Table 1—Continued

	6A	2001 Dec 14	24
SGRSC J2228−5600	6D	2001 Nov 26	21
	6A	2001 Dec 14	24
SGRSC J2253−5813	6D	2001 Nov 26	21
	6A	2001 Dec 14	24
SGRSC J2336−8151	6D	2001 Nov 26	28
	6A	2001 Dec 14	24

Table 2. Journal of ATCA observations-4.8 GHz

Name	Array	Date	Time (min)
SGRSC J0020−7321	6A	2002 Nov 22	227
SGRS J0326−7730	6A	2002 Nov 22	268
SGRSC J0622−5938	6A	2002 Nov 22	152
SGRS J0810−6800	6A	2002 Nov 22	160
	6C	2004 May 15	160
SGRS J1259−7737	6A	2002 Nov 22	170

Table 3. Journal of optical spectroscopy observations-I

Name	Magnitude (b_j)	Date	Exposure (s)
SGRS J0047−8307	20.2	2002 Aug 04	2000
		2002 Nov 05	2000
SGRSC J0129−6433	18.5	2002 Aug 02	2000
SGRS J0237−6429	20.9	2002 Aug 04	2000
		2002 Nov 03	2000
SGRS J0331−7710	18.2	2002 Aug 04	2000
		2002 Nov 04	2000
SGRS J0400−8456	16.9	2002 Nov 04	2000
		2002 Nov 05	2000
SGRS J0631−5405	16.9	2002 Nov 04	2000
SGRS J0746−5702	18	2002 Nov 04	2000
SGRS J0810−6800	–	2002 Nov 05	2000
SGRS J0843−7007	17.7	2002 Nov 05	2000
SGRS J1336−8019	16.7	2002 Aug 03	2000
SGRS J1728−7237	21	2002 Aug 01	2000
		2002 Aug 02	2000
SGRS J1911−7048	19.4	2002 Nov 05	2000
SGRS J1946−8222	22.3	2002 Aug 04	2000
SGRSC J2228−5600	17.5	2002 Aug 02	2000

Table 4. Journal of optical spectroscopy observations-II

Name	Magnitude (b_j)	Date	Exposure (s)
SGRS J0237−6429	20.9	2004 Sep 13	2×1500
SGRS J0326−7730	20.7	2004 Sep 13	2×1500
SGRS J0810−6800	16.3	2004 Apr 15	4×2000
SGRS J1259−7737	22.4	2004 Apr 15	5×2000
SGRS J1911−7048	19.4	2004 Apr 14	3×2000
SGRS J1946−8222	22.3	2004 Apr 14	4×2000

Table 5. Observed properties of the sample of 18 SUMSS giant radio sources

Name	Redshift	Angular size (arcmin)	Radio structure FR-I/FR-II	Total flux density $S_{tot}^{843\ \mathrm{MHz}}$ (mJy)
SGRS J0047−8307	0.2591	5.6	FR-II	543
SGRS J0143−5431	0.1791	5.5	FR-II	217
SGRS J0237−6429	0.364:	6.6	FR-II	145
SGRS J0326−7730	0.2771	5.3	FR-II	357
SGRS J0331−7710	0.1456	17.7	FR-II	687
SGRS J0400−8456	0.1037	6.3	FR-I	175
SGRS J0515−8100	0.1050	7.5	FR-I/FR-II	264
SGRS J0631−5405	0.2036	5.2	FR-II	694
SGRS J0746−5702	0.1300	5.5	FR-I	194
SGRS J0810−6800	0.2311	6.5	FR-II	271
SGRS J0843−7007	0.1381	5.6	FR-I	203
SGRS J1259−7737	> 0.3[a]	5.7	FR-II	439
SGRS J1336−8019	0.2478	10.1	FR-II	483
SGRS J1728−7237	0.4735	6.2	FR-II	214
SGRS J1911−7048	0.2152	6.0	FR-II	238
SGRS J1919−7959	0.3462	6.0	FR-II	1262
SGRS J1946−8222	0.333:	7.4	FR-II	219
SGRS J2159−7219	0.0974	9.2	FR-II	142

[a]Redshift lower limit is using K=16.2 ±0.2 mag. See Section 5.1.12.

Table 6. Results of ATCA observations of the giant radio source sample

Name	Other names	Associated SUMSS sources	Core position RA & DEC (J2000 epoch)	Core flux density (mJy) 1.4 GHz	4.8 GHz
SGRS J0047−8307	PKS B0046−833	J004756−830816	00 47 55.5 −83 08 12.5	8.3	
	PMN J0047−8307	J004704−830722			
	MRC 0046−833	J004931−830914			
SGRS J0143−5431		J014344−543140	01 43 43.2 −54 31 39.0	1.7	
		J014353−543249			
		J014335−542919			
SGRS J0237−6429	PMN J0237−6428	J023655−642751	02 37 09.9 −64 30 02.2	2.0	
		J023728−643246			
SGRS J0326−7730	PMN J0326−7730	J032514−772928	03 26 01.3 −77 30 16.9	–	0.46
		J032506−772809			
		J032618−773039			
SGRS J0331−7710	PKS B0333−773	J033133−771133	03 31 39.8 −77 13 19.3	1.3	
	PMN J0331−7709	J033135−770900			
	PMN J0331−7719	J033138−772218			
SGRS J0400−8456	PMN J0401−8457	J040116−845642	04 01 18.4 −84 56 35.9	2.9	
		J040058−845449			
		J040058−845829			
		J035945−845530			
		J040145−850015			
SGRS J0515−8100	PMN J0515−8101	J051541−810139	05 15 55.0 −80 59 44.4	3.06	
		J051611−810219			
		J051653−810128			
		J051548−810314			
SGRS J0631−5405	PMN J0631−5405	J063159−540506	06 32 01.0 −54 04 58.7	37.7	
	MRC 0630−540	J063214−540405			
	1WGA J0631.9−5404	J063222−540320			

Table 6—Continued

		J063151−540540			
SGRS J0746−5702	PMN J0746−5703	J074615−570312	07 46 18.6 −57 02 59.1	36.4	
	PMN J0746−5702	J074631−570152			
	PMNM 074521.2−565530	J074602−570434			
SGRS J0810−6800	PMN J0810−6759	J081038−675911	08 10 55.1 −68 00 07.7	–	0.34
		J081121−680109			
		J081029−675855			
		J081131−680200			
SGRS J0843−7007	PMN J0843−7006	J084243−700653	08 43 05.9 −70 06 55.6	12.0	
		J084305−700655			
		J084331−700739			
		J084349−700729			
SGRS J1259−7737	PKS B1255−773	J125846−773924	12 59 09.0 −77 37 28.4	–	0.33
	PMN J1259−7736	J125931−773500			
		J125920−773623			
SGRS J1336−8019	PMN J1335−8016	J133600−801807	13 35 59.7 −80 18 05.1	8.6	
	PMN J1336−8022	J133601−801637			
		J133600−801428			
		J133624−802250			
SGRS J1728−7237	PMN J1728−7237	J172828−723732	17 28 28.1 −72 37 34.9	11.9	
		J172806−723549			
		J172859−724011			
SGRS J1911−7048		J191052−704906	19 10 55.2 −70 49 00.9	1.2	
		J191120−704716			
		J191025−705110			
SGRS J1919−7959	PKS B1910−800	J191903−795741	19 19 16.9 −79 59 34.9	2.6	
	PMN J1918−7957	J191932−800145			
	MRC 1910−800	J191856−795651			

Table 6—Continued

SGRS J1946−8222	PMN J1946−8221	J194640−822234	19 46 50.5 −82 22 53.8	2.1
		J194552−822037		
		J194818−822539		
SGRS J2159−7219	PMN J2159−7220	J215908−721904	21 59 10.1 −72 19 06.6	9.6
		J215918−722013		
		J215947−722203		
		J215827−721528		

Table 7. Redshifts and spectral lines

Name	Redshift	Prominent lines
SGRS J0047−8307	0.2591±0.0002	Absorption lines: FeI4384, Hβ, Mgb
SGRS J0143−5431	0.1791±0.0001	Weak emission line: [OII]3727
		Absorption lines: K, H, G, Hβ, Mgb
SGRS J0237−6429	0.364:	Weak emission lines: [OIII]4959,5007
		Possible absorption line: Hβ
SGRS J0326−7730	0.2771±0.0002	Moderate strength emission lines: [OIII]4959,5007
		Absorption lines: K+H
SGRS J0331−7710	0.1456±0.0001	Absorption lines: Mgb and Na
SGRS J0400−8456	0.1037±0.0003	Absorption lines: Mgb, Ca+Fe, and Na
SGRS J0515−8100	0.1050±0.0002	Weak emission lines: Hα, [NII]6583 and [SII]6716,6731
		Absorption lines: Mgb, FeI and Na
SGRS J0631−5405	0.2036±0.0001	Quasar. Broad emission lines: Hβ, Hα
		Narrow emission lines: [OIII]4959,5007
SGRS J0746−5702	0.1300±0.0005	Absorption lines: Mgb and Na
SGRS J0810−6800	0.2311±0.0002	Quasar. Broad emission lines: Hγ, Hβ and Hα
		Narrow emission lines: [OIII]4363, [OIII]4959,5007
SGRS J0843−7007	0.1381±0.0003	Absorption lines: Mgb and Na
SGRS J1336−8019	0.2478±0.0001	Weak emission lines: [OIII]4959,5007
SGRS J1728−7237	0.4735±0.0002	Strong narrow emission lines: [OIII]4959,5007
		Weak emission lines: [OII]3727, Hβ
		Absorption line: G
SGRS J1911−7048	0.2152±0.0001	Absorption lines:Hδ, G, Mgb, Ca+Fe and Na
SGRS J1919−7959	0.3462±0.0002	Narrow emission lines: [OIII]4959,5007 and possible [SII]6716,6731
SGRS J1946−8222	0.333:	Absorption lines: G and Mgb
SGRS J2159−7219	0.0974±0.0001	Absorption lines: K, H, G, Mgb and Na

Table 8. Derived properties of the SUMSS giant radio sources

Name	Redshift	Linear size (Mpc)	1.4-GHz core power (10^{24} W Hz^{-1})	843-MHz total power (10^{26} W Hz^{-1})	M_b
SGRS J0047−8307	0.2591	1.34	1.7	1.1	−20.3
SGRS J0143−5431	0.1791	0.99	0.15	0.19	−20.6
SGRS J0237−6429	0.364:	2.24	0.9	0.64	−20.5
SGRS J0326−7730	0.2771	1.68	0.11[a]	0.84	−20.0
SGRS J0331−7710	0.1456	2.67	0.07	0.38	−21.0
SGRS J0400−8456	0.1037	0.71	0.08	0.05	−21.5
SGRS J0515−8100	0.1050	0.86	0.08	0.07	−21.1
SGRS J0631−5405	0.2036	1.03	4.4	0.81	−23.1
SGRS J0746−5702	0.1300	0.76	1.6	0.08	−20.9
SGRS J0810−6800	0.2311	1.28	0.05[a]	0.42	−23.9
SGRS J0843−7007	0.1381	0.81	0.6	0.10	−21.3
SGRS J1259−7737	> 0.3	> 1.5	> 0.09	> 1.25	< -18.5[b]
SGRS J1336−8019	0.2478	2.34	1.57	0.88	−23.7:[c]
SGRS J1728−7237	0.4735	2.2	9.95	1.79	≤ -21.1[d]
SGRS J1911−7048	0.2152	1.24	0.16	0.32	−20.7
SGRS J1919−7959	0.3462	1.75	1.03	5.00	≤ -19.3[e]
SGRS J1946−8222	0.333:	2.14	0.76	0.80	≤ -18.9[e]
SGRS J2159−7219	0.0974	0.98	0.22	0.03	−21.6

[a]The core luminosity given for SGRS J0326−7730 and J0810−6800 is using 4.8-GHz core flux and assuming flat core spectral index.

[b]Redshift lower limit is based on K=16.2±0.2 mag and using K-z relation for radio galaxies. The core luminosity is using 4.8-GHz core flux and assuming flat core spectral index. The host galaxy is obscured; this is reflected in its absolute magnitude.

[c]The host galaxy is in a close pair in which the objects appear equally bright; the object to the north is a star. The galaxy magnitude taken from Table 3 has been estimated by dividing the integrated magnitude equally between the two objects.

[d]The host galaxy of SGRS J1728−7237 is partly obscured by a star. The absolute magnitude is based on apparent magnitude judged from the neighbourhood galaxies within 5″. The galaxy is likely

to be more luminous.

[e]The host galaxies for SGRS J1919−7959 and J1946−8222 are obscured. This is reflected in their absolute magnitudes.

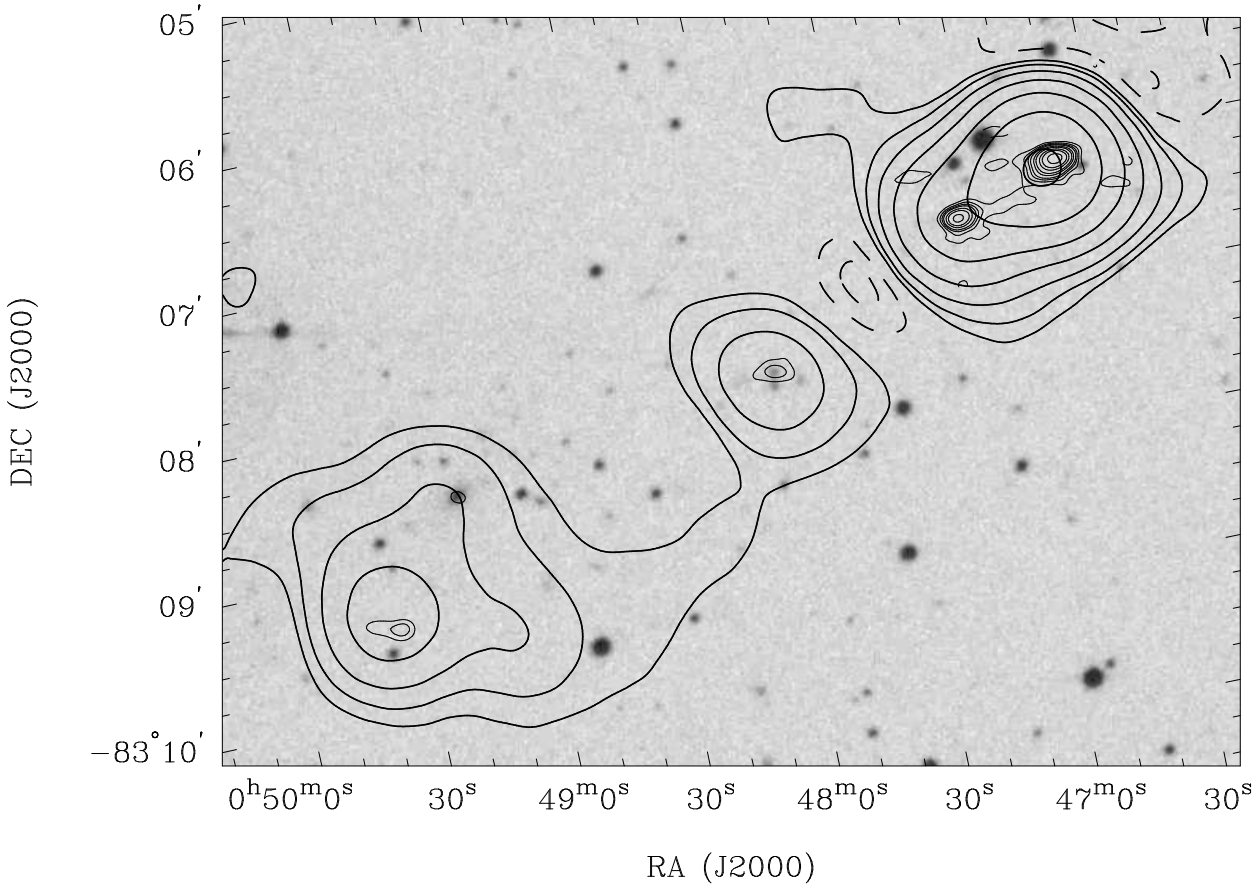

Fig. 1.— SGRS J0047−8307. Radio-optical overlays for the SUMSS giant radio sources are shown in this and the following 17 figures. 843 MHz contours for the low resolution SUMSS images are shown in thick lines and 1.4-GHz (4.8 GHz where specified) contours for the higher resolution ATCA images are shown using thin lines. The radio contours are overlaid on the red SSS optical field shown using grey scales. Contours are at (−2, −1, 1, 2, 4, 8, 16 32, 64) × 4 mJy beam^{-1} for SUMSS and at (−2, −1, 1, 2, 3, 4, 6, 8, 12, 16, 24) × 3 mJy beam^{-1} for ATCA. The beams have FWHM 45.″2 × 45″ (SUMSS) and 8.″6 × 5.″9 (ATCA).

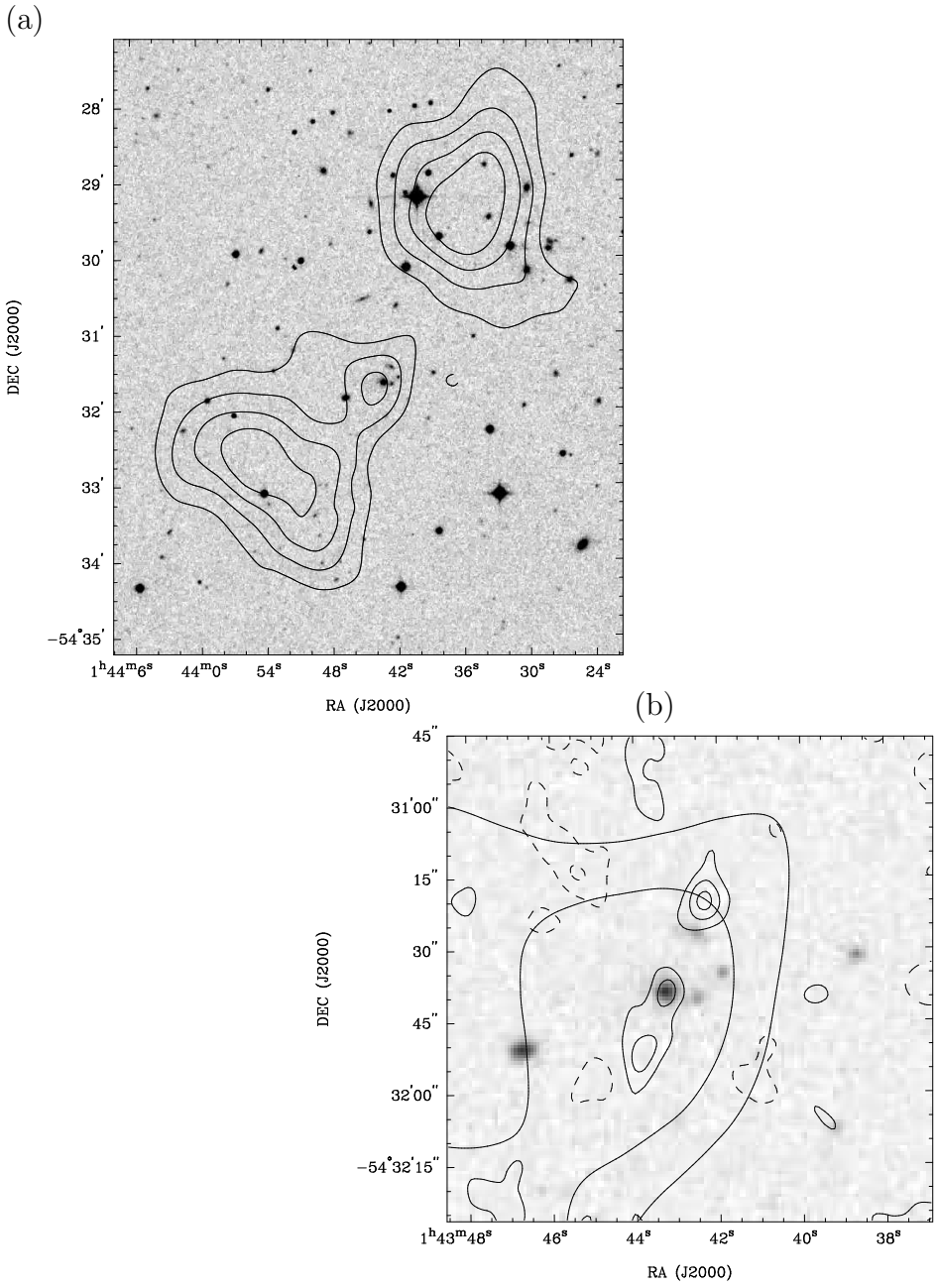

Fig. 2.— SGRS J0143−5431 radio contours on blue SSS grey scale. SUMSS contours (thick lines) at (−2, −1, 1, 2, 3, 4) × 4 mJy beam^{-1} and ATCA contours (thin lines) at (−2, −1, 1, 2, 3) × 0.7 mJy beam^{-1}. Panel (b) shows a zoom of the region close to the core. The beams have FWHM 54.″3 × 45″ (SUMSS) and 8.″5 × 7.″2 (ATCA).

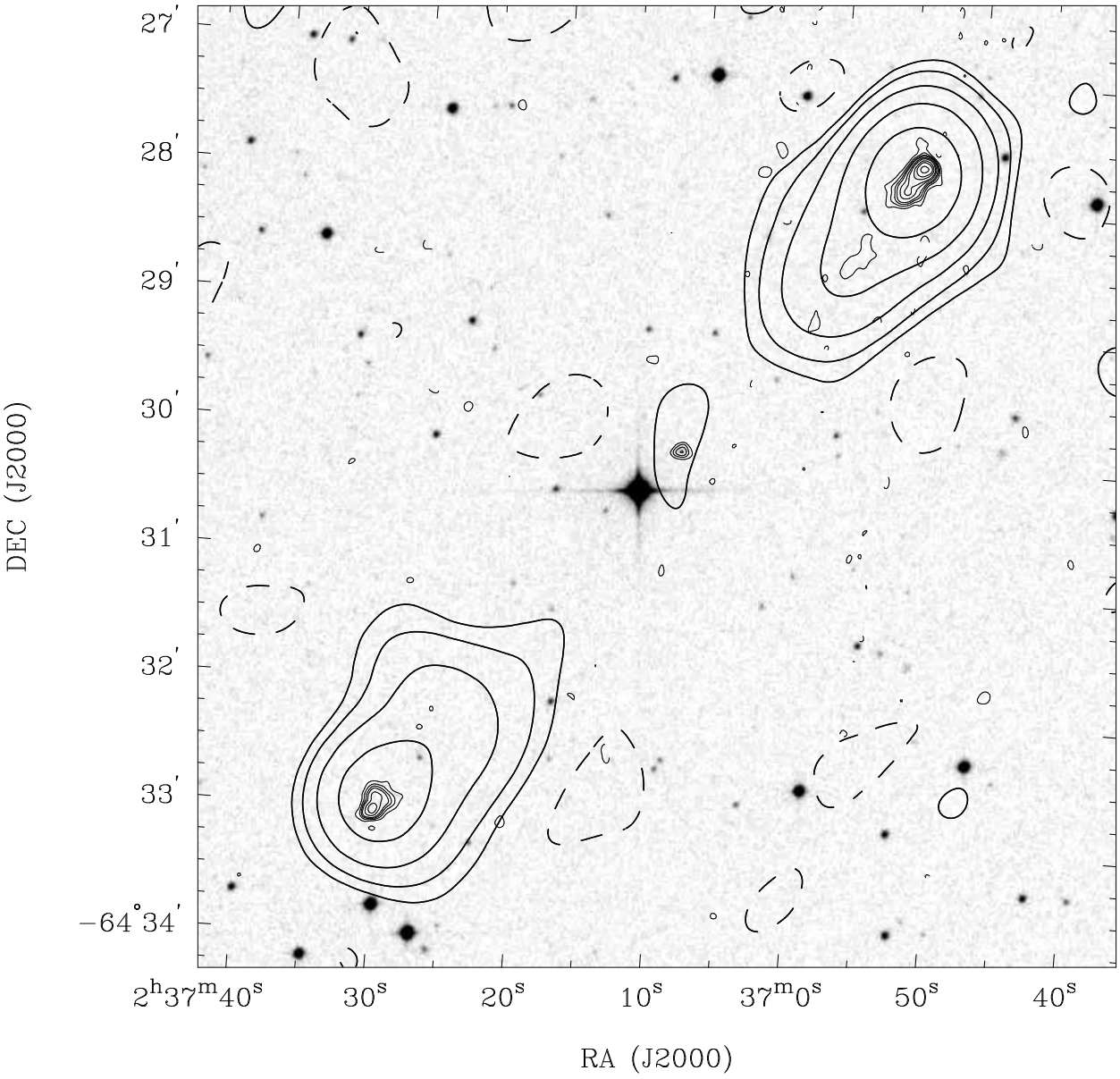

Fig. 3.— SGRS J0237−6429 radio contours on blue SSS grey scale. SUMSS contours (thick lines) at (−2, −1, 1, 2, 4, 8, 16) × 2 mJy beam^{-1} and ATCA contours (thin lines) at (−2, −1, 1, 2, 3, 4, 6, 8, 12, 16, 24) × 2 mJy beam^{-1}. The beams have FWHM 50.″1 × 45″ (SUMSS) and 7.″6 × 7.″3 (ATCA).

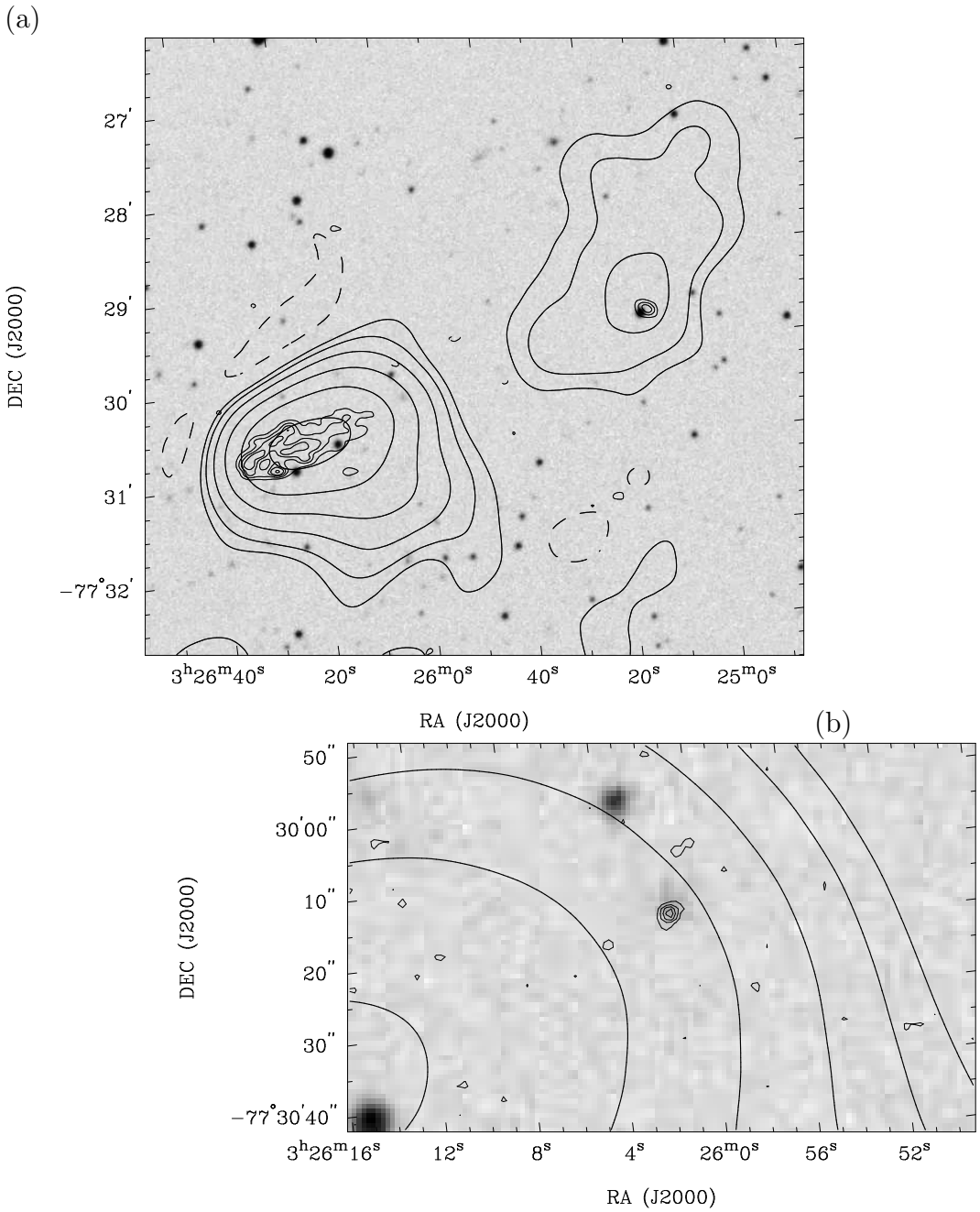

Fig. 4.— SGRS J0326−7730 radio contours on red SSS grey scale. A zoom of the core region is in panel (b) in which 4.8-GHz ATCA contours are shown in thin lines. SUMSS contours (thick lines) are at (−2, −1, 1, 2, 4, 8, 16, 32) × 3 mJy beam^{-1} and ATCA contours (thin lines) are at (−2, −1, 1, 2, 3, 4, 6) × 0.7 mJy beam^{-1} for the 1.4-GHz image and at (−2, −1, 1, 2, 3, 4) × 0.1 mJy beam^{-1} for the 4.8-GHz image. The beams have FWHM 46.″4 × 45″ (SUMSS), 7.″8 × 4.″9 (ATCA, 1.4 GHz) and 2.″2 × 1.″8 (ATCA, 4.8 GHz).

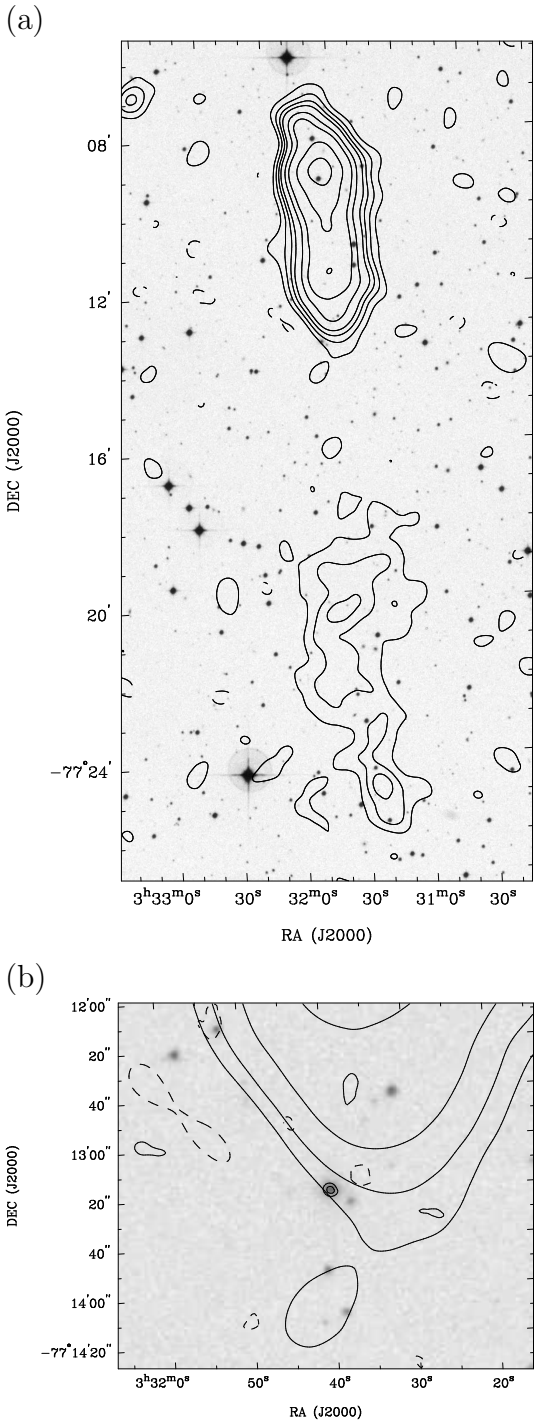

Fig. 5.— SGRS J0331−7710 radio contours on blue SSS grey scale. A zoom of the core region is in panel (b). SUMSS contours (thick lines) are at (−2, −1, 1, 2, 3, 4, 6, 8, 12, 16) × 2 mJy beam^{-1} in panel (a) and at (−1, 1, 2, 4, 8) × 3 mJy beam^{-1} in panel (b); ATCA contours (thin lines) are at (−1, 1, 1.5) × 0.8 mJy beam^{-1}. The beams have FWHM 46.″4 × 45″ (SUMSS) and 9.″1 × 6″ (ATCA).

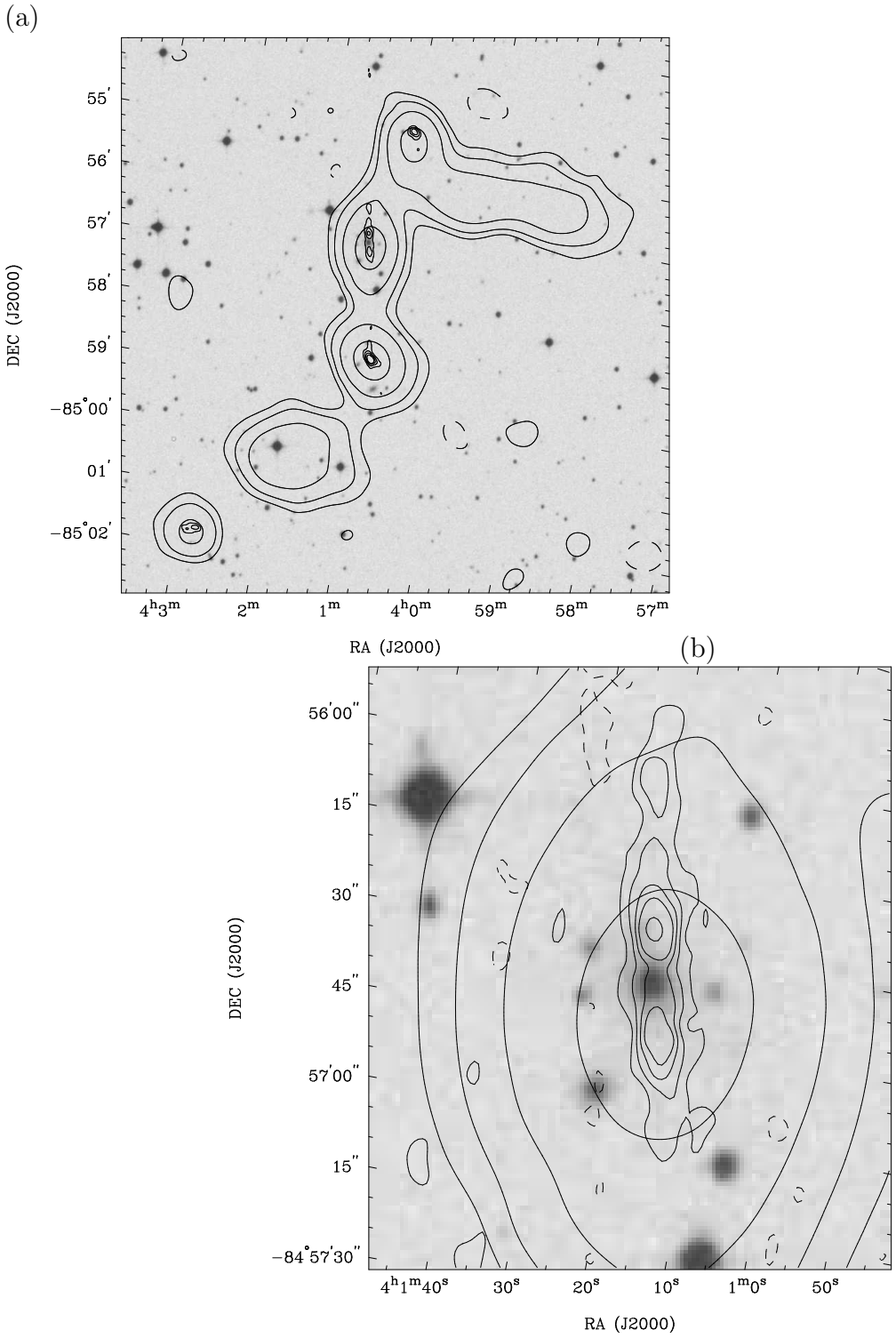
(a)
55′
56′
57′
58′
59′
−85°00′
01′
−85°02′
DEC (J2000)
4h3m
2m
1m
4h0m
59m
58m
57m
RA (J2000)
(b)
56′00″
15″
30″
45″
57′00″
15″
−84°57′30″
DEC (J2000)
4h1m40s
30s
20s
10s
1m0s
50s
RA (J2000)

(c)

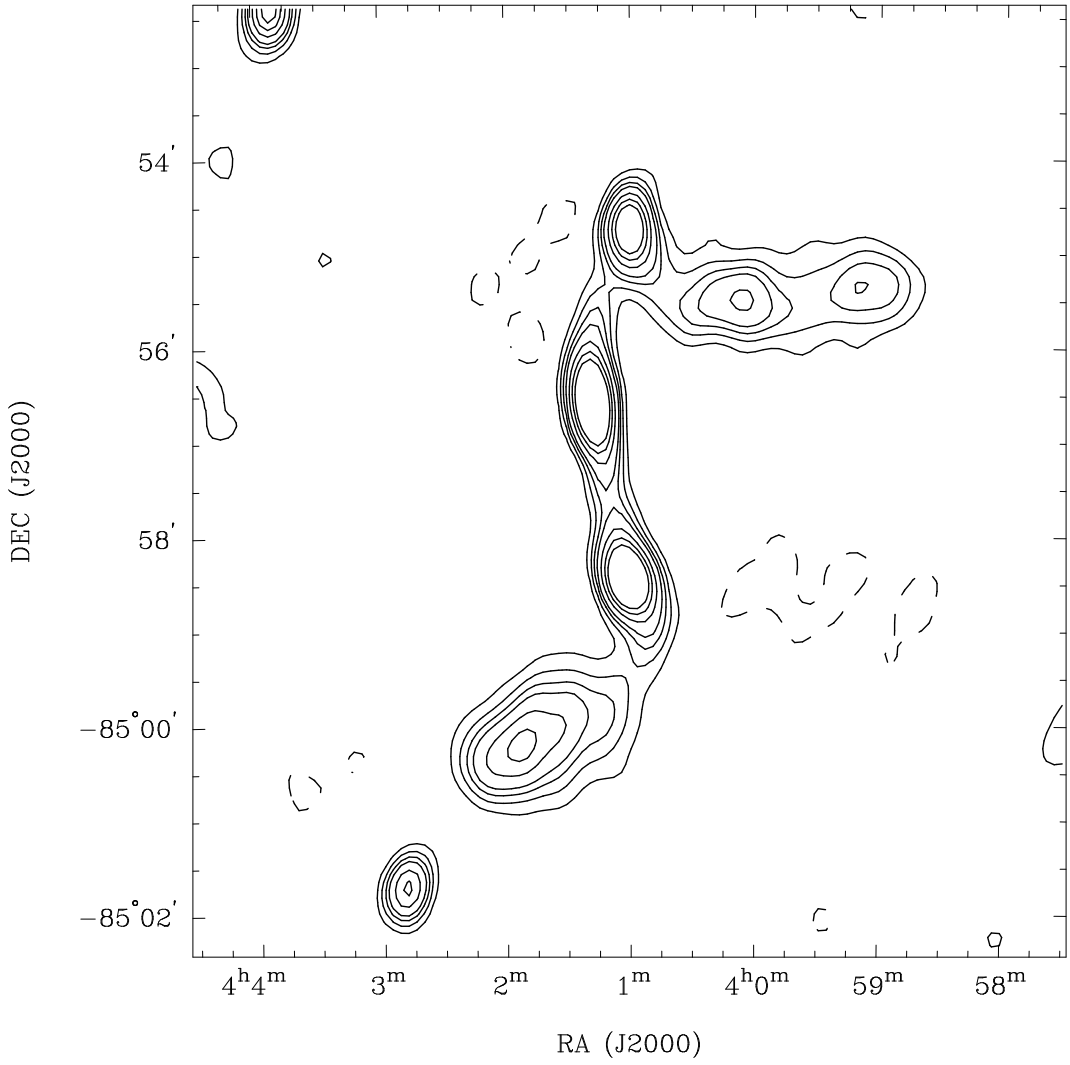

Fig. 6.— SGRS J0400−8456 radio contours on blue SSS grey scale. A zoom of the core region is in panel (b). SUMSS contours (thick lines) are at (−1, 1, 2, 4, 8) × 2 mJy beam^{-1} in panel (a) and at (−1, 1, 2, 4, 8) × 3 mJy beam^{-1} in panel (b); ATCA contours (thin lines) are at (−1, 1, 2, 3, 4) × 1 mJy beam^{-1} in panel (a) and at (−1, 1, 2, 3, 4, 6) × 0.1 mJy beam^{-1} in panel (b). The beams have FWHM 45.″2 × 45″ (SUMSS) and 8.″1 × 4.″7 (ATCA).Low-resolution 1.4-GHz ATCA image of SGRS J0400−8456. The contours are at (−2, −1, 1, 2, 3, 4, 6, 8, 10)× 0.8 mJy beam^{-1}. The beam FWHM is 34″ × 21″.

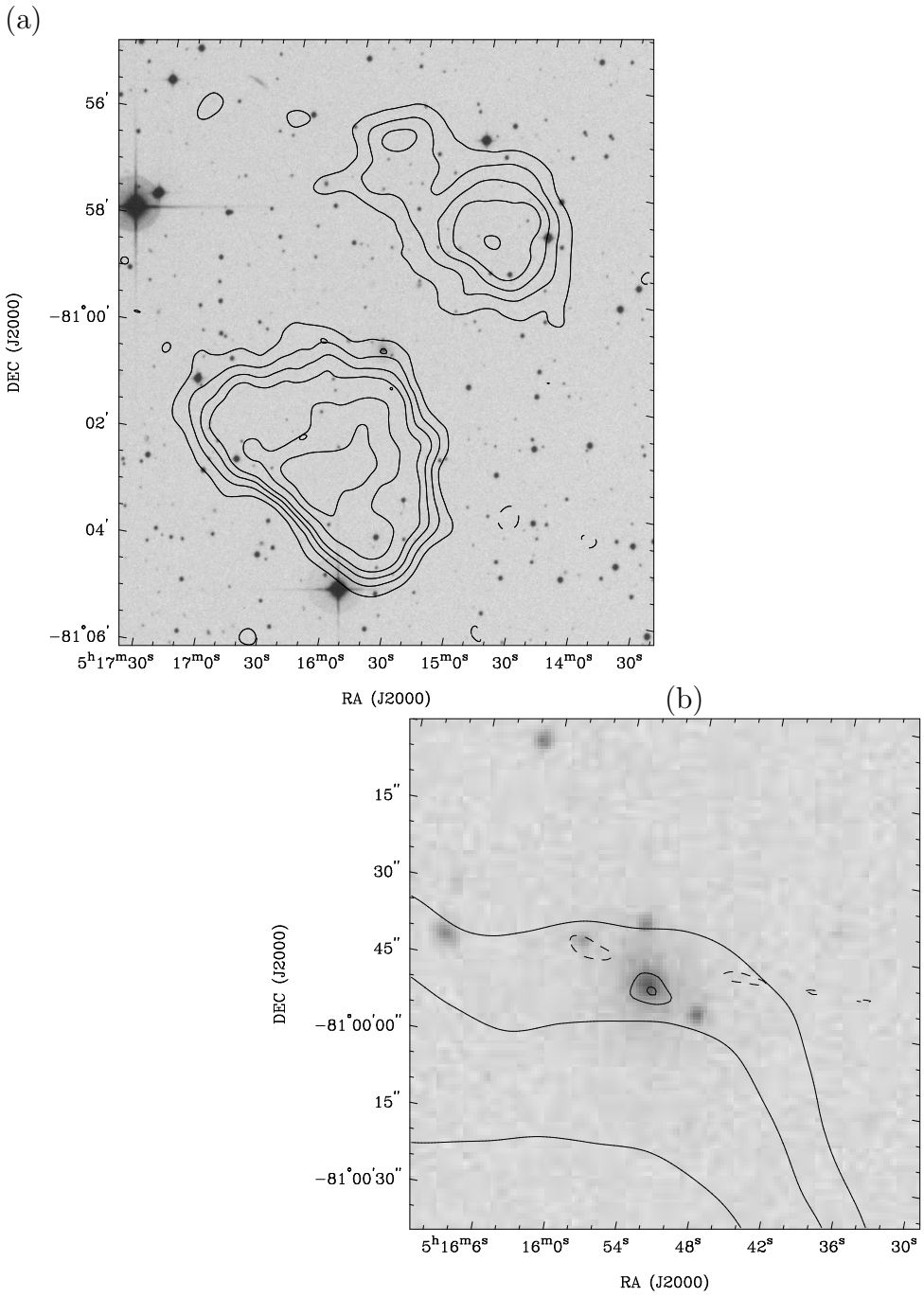

Fig. 7.— SGRS J0515−8100 radio contours on blue SSS grey scale. A zoom of the core region is in panel (b). SUMSS contours (thick lines) are at (−1, 1, 2, 3, 4, 6, 8) × 1.5 mJy beam^{-1}, ATCA contours (thin lines) are at 2 mJy beam^{-1} in panel (a) and at (−1, 1, 2) × 1 mJy beam^{-1} in panel (b). The beams have FWHM 45.″7 × 45″ (SUMSS), 8.″5 × 6.″1 (ATCA image in panel (a)) and 7.″1 × 5″ (ATCA image in panel (b)).

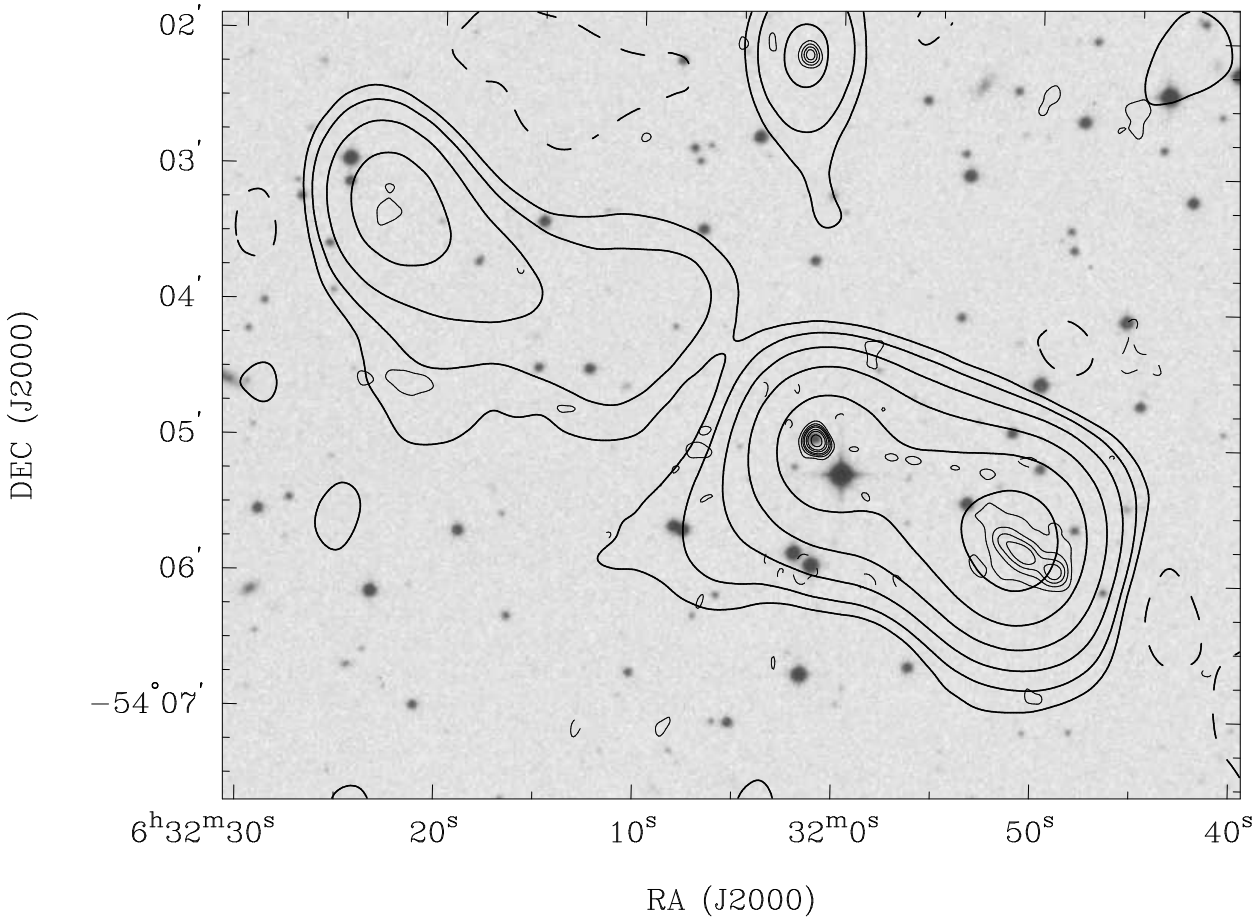

Fig. 8.— SGRS J0631−5405 radio contours on blue SSS grey scale. SUMSS contours (thick lines) are at (−1, 1, 2, 4, 8, 16, 32) × 4 mJy beam^{-1} and ATCA contours (thin lines) are at (−1, 1, 2, 3, 4, 6, 8, 12) × 2.5 mJy beam^{-1}. The beams have FWHM 54.″3 × 45″ (SUMSS) and 8.″5 × 7.″3 (ATCA).

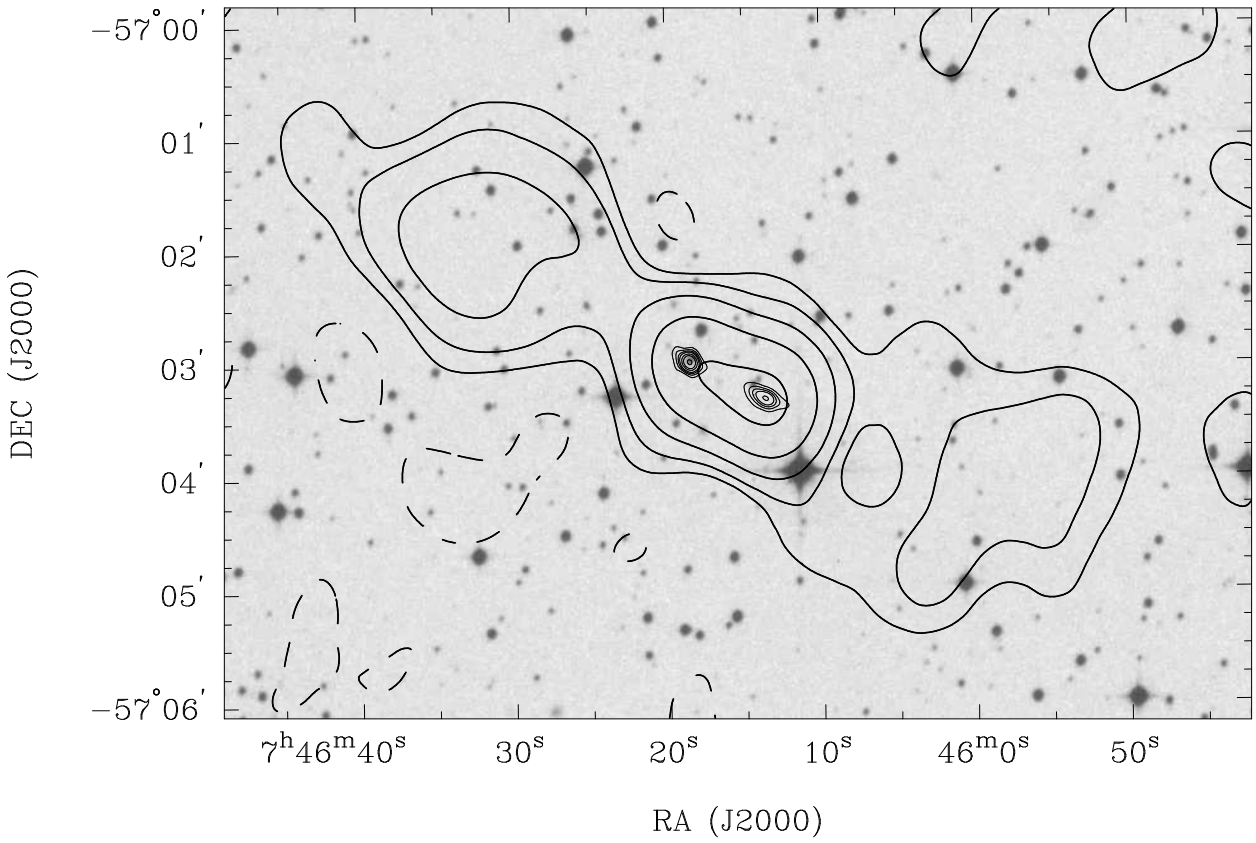

Fig. 9.— SGRS J0746−5702 radio contours on blue SSS grey scale. SUMSS contours (thick lines) are at (−1, 1, 2, 4, 8, 16) × 3 mJy beam^{-1} and ATCA contours (thin lines) are at (−1, 1, 2, 3, 4, 6, 8, 12) × 3 mJy beam^{-1}. The beams have FWHM 54.″3 × 45″ (SUMSS) and 8.″4 × 7.″1 (ATCA).

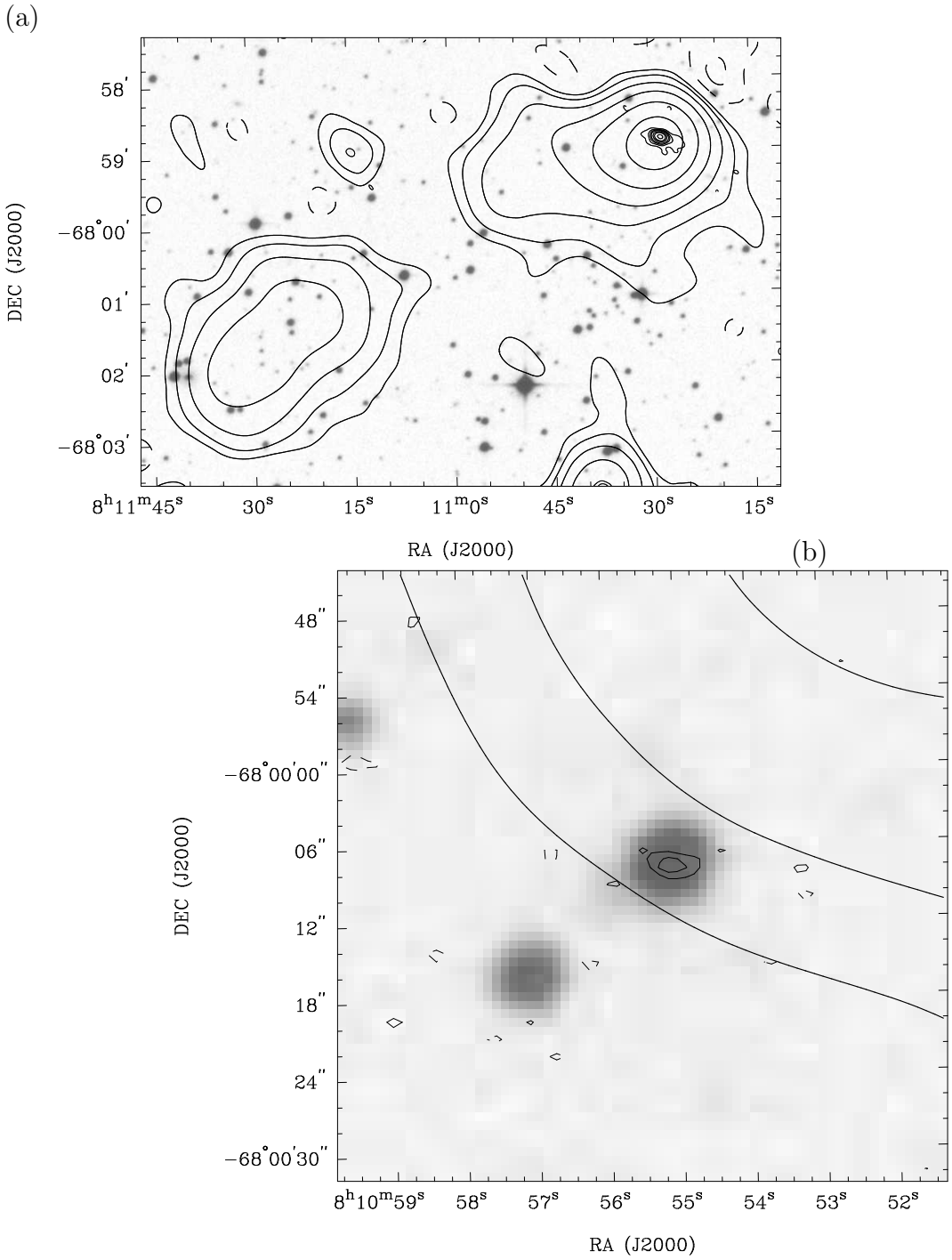

Fig. 10.— SGRS J0810−6800 radio contours on red SSS grey scale. The core region is shown in panel (b) with 4.8-GHz contours plotted in thin lines. SUMSS contours (thick lines) are at (−1, 1, 2, 4, 8, 16, 32) × 1.5 mJy beam^{-1}. ATCA contours (thin lines) are at (−1, 1, 2, 3, 4, 6, 8, 12) × 1.5 mJy beam^{-1} for the 1.4-GHz image and at (−1, 1, 2) × 0.1 mJy beam^{-1} for the 4.8-GHz image. The beams have FWHM 48.″5 × 45″ (SUMSS), 9.″3 × 6.″1 (ATCA 1.4 GHz) and 3.″4 × 1.″4 (ATCA 4.8 GHz).

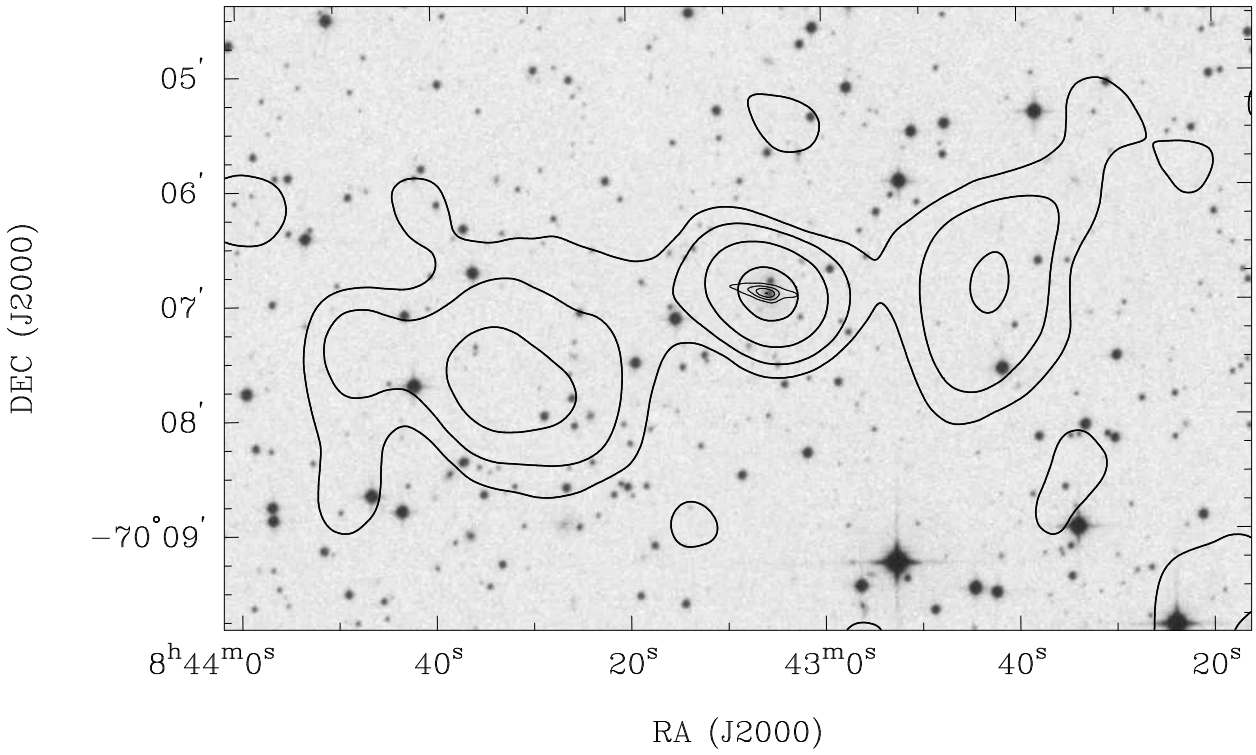

Fig. 11.— SGRS J0843−7007 radio contours on blue SSS grey scale. SUMSS contours (thick lines) are at (−1, 1, 2, 4, 8) × 3 mJy beam^{-1} and ATCA contours (thin lines) are at (−1, 1, 2, 3, 4) × 3 mJy beam^{-1}. The beams have FWHM 47.″3 × 45″ (SUMSS) and 9.″5 × 6″ (ATCA).

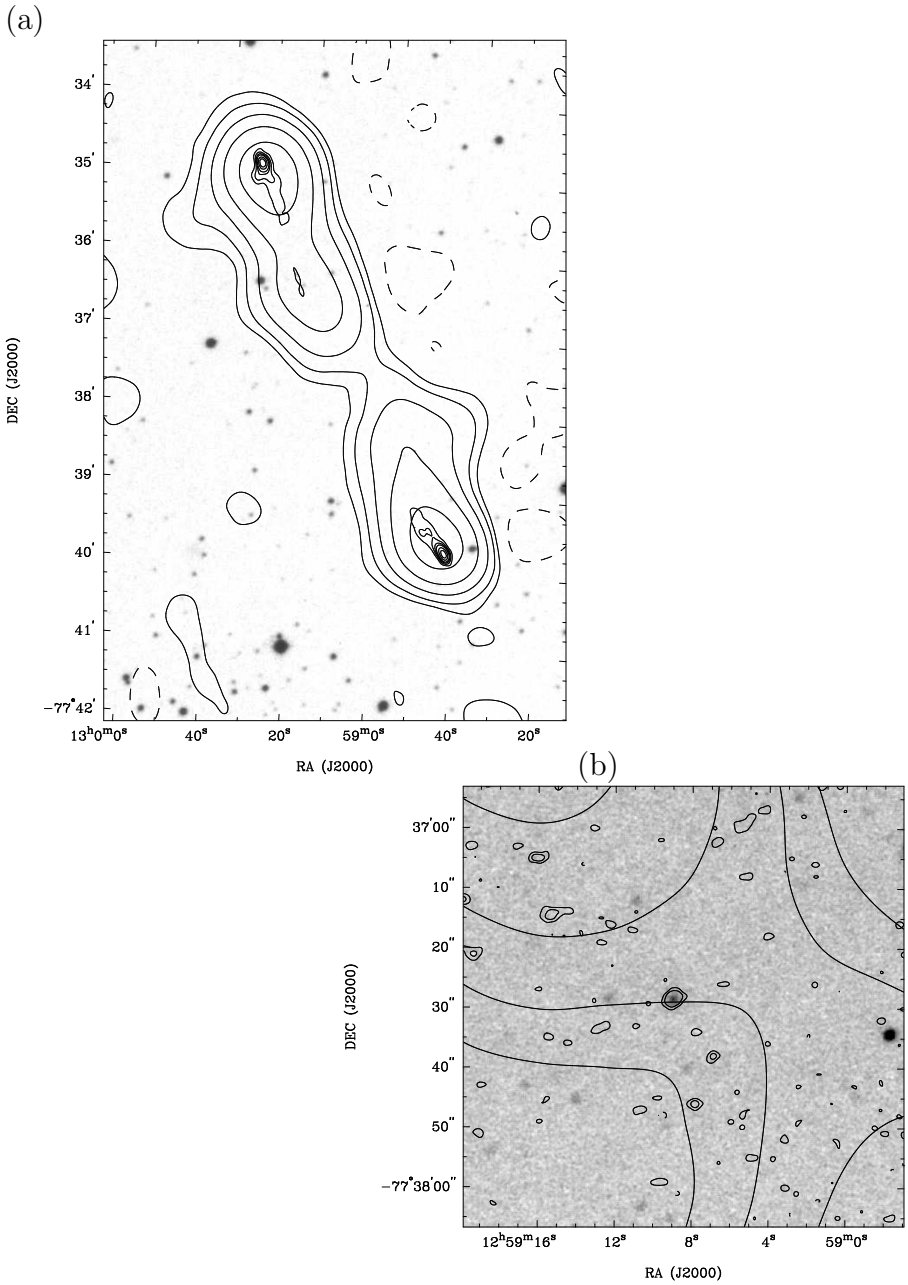

Fig. 12.— SGRS J1259−7737 radio contours. Blue SSS grey scale image is in panel (a) and SSO 2.3 m K-band image in grey scale is in panel (b). The K-band image was obtained by Helen Johnston. The core region is shown in panel (b) with 4.8-GHz contours shown using thin lines. SUMSS contours (thick lines) are at (−1, 1, 2, 4, 8, 16) × 4 mJy beam^{-1}, ATCA contours (thin lines) are at (−1, 1, 2, 3, 4, 6, 8) × 3 mJy beam^{-1} for the 1.4-GHz image and at (−1, 1, 2) × 0.07 mJy beam^{-1} for the 4.8-GHz image. The beams have FWHM 46.″4 × 45″ (SUMSS), 9.″4 × 5.″8 (ATCA 1.4 GHz) and 2.″2 × 1.″8 (ATCA 4.8 GHz).

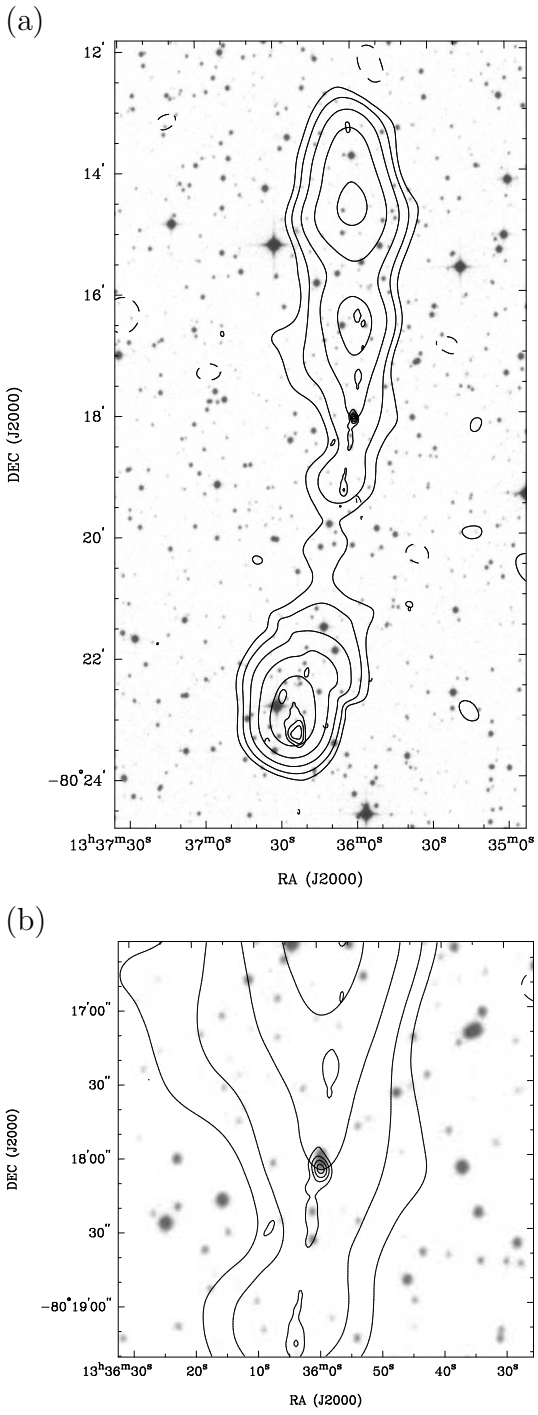

Fig. 13.— SGRS J1336−8019 radio contours on blue SSS grey scale. A zoom of the core region is in panel (b). SUMSS contours (thick lines) are at $(-1, 1, 2, 4, 8, 16) \times 3$ mJy beam^{-1} and ATCA contours (thin lines) are at $(-1, 1, 2, 3, 4) \times 2$ mJy beam^{-1}. The beams have a FWHM $45\farcs7 \times 45''$ (SUMSS) and $9\farcs3 \times 5\farcs8$ (ATCA).

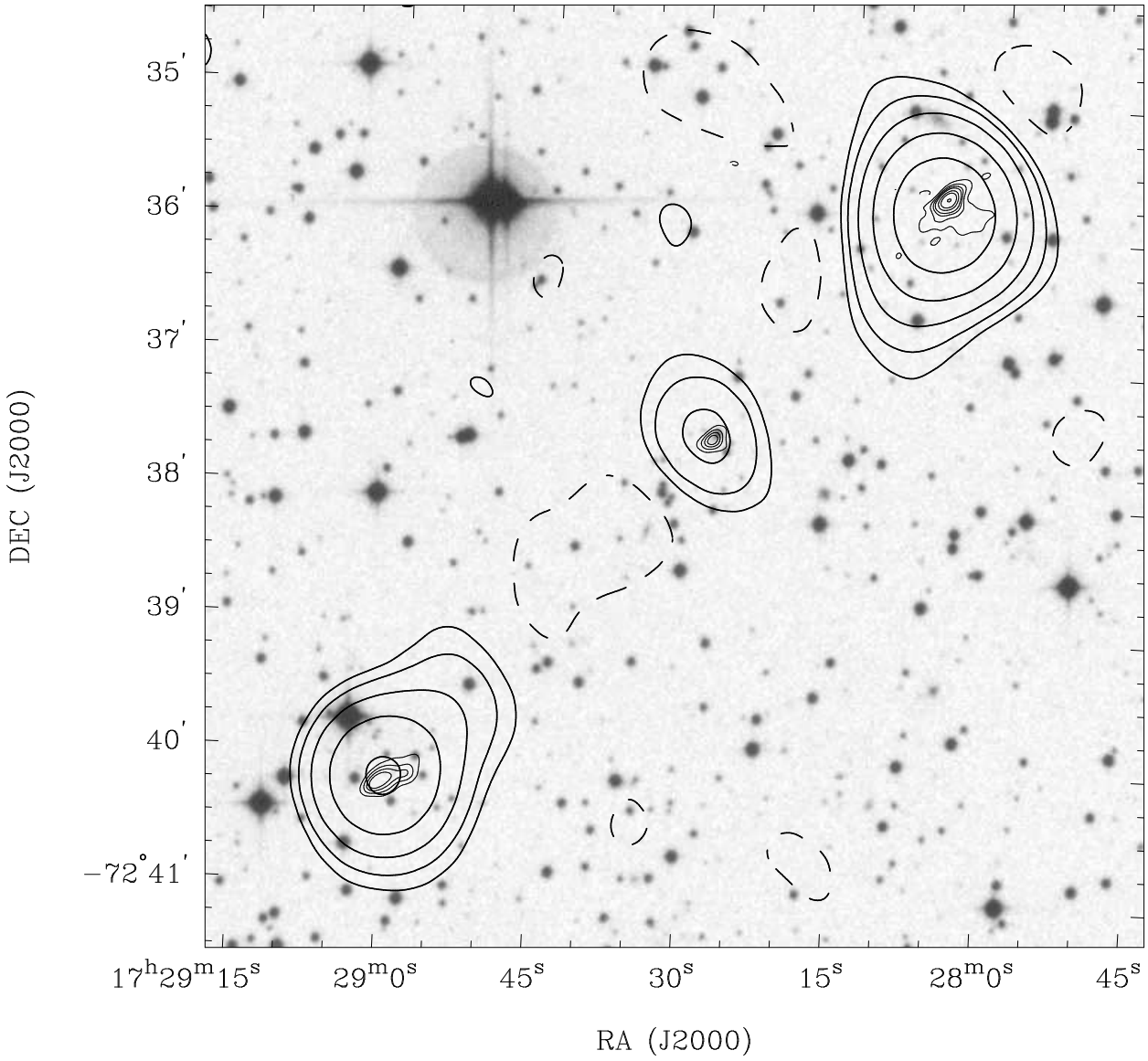

Fig. 14.— SGRS J1728−7237 radio contours on blue SSS grey scale. SUMSS contours (thick lines) are at (−1, 1, 2, 4, 8, 16) × 3 mJy beam^{-1} and ATCA contours (thin lines) are at (−1, 1, 2, 3, 4, 6, 8, 12) × 2.5 mJy beam^{-1}. The beams have FWHM 47.″3 × 45″ (SUMSS) and 8.″9 × 6.″1 (ATCA).

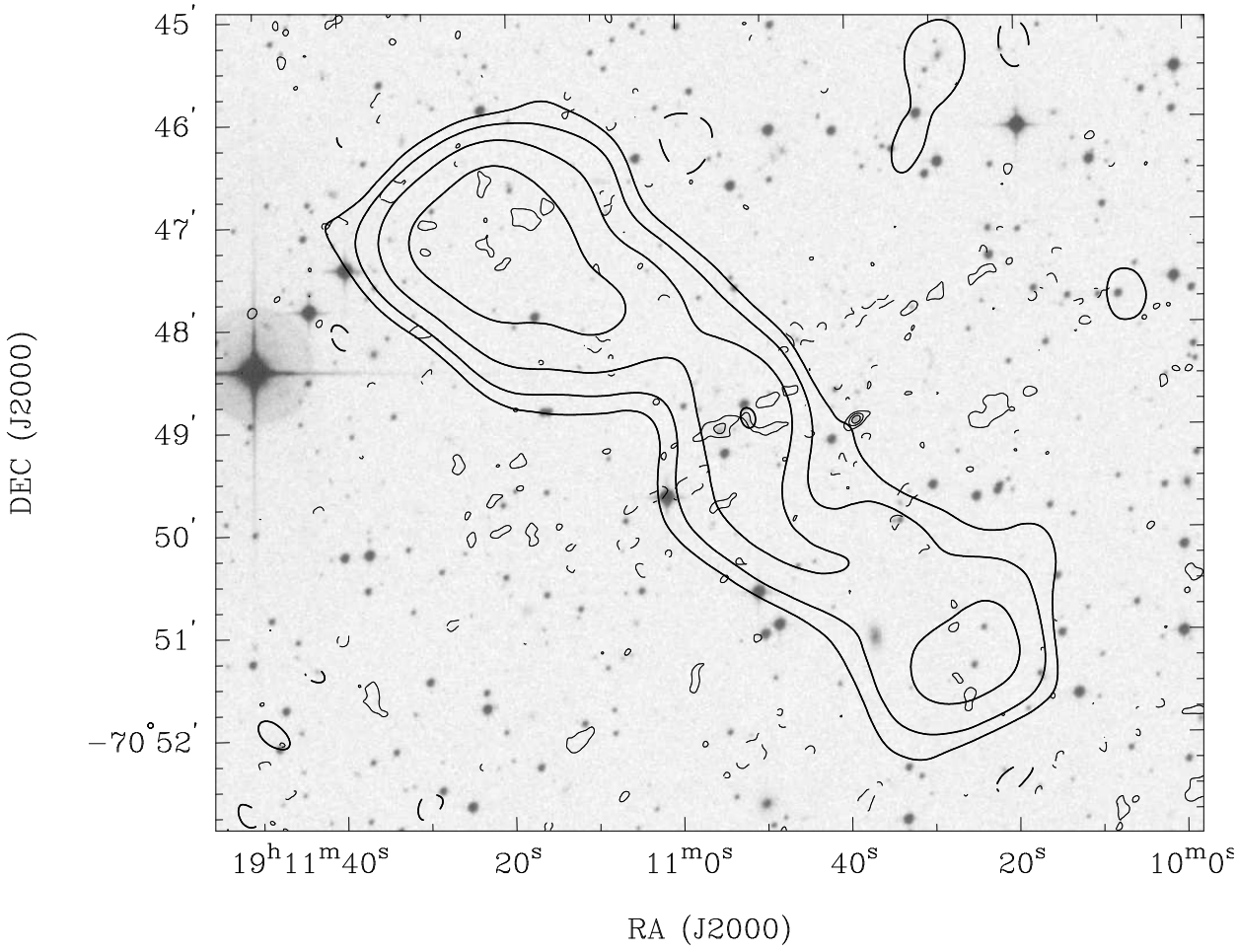

Fig. 15.— SGRS J1911−7048 radio contours on blue SSS grey scale. SUMSS contours (thick lines) are at (−1, 1, 2, 4, 8) × 2 mJy beam^{-1} and ATCA contours (thin lines) are at (−1, 1, 2) × 0.5 mJy beam^{-1}. The beams have FWHM 47.″3 × 45″ (SUMSS) and 9.″8 × 5.″9 (ATCA).

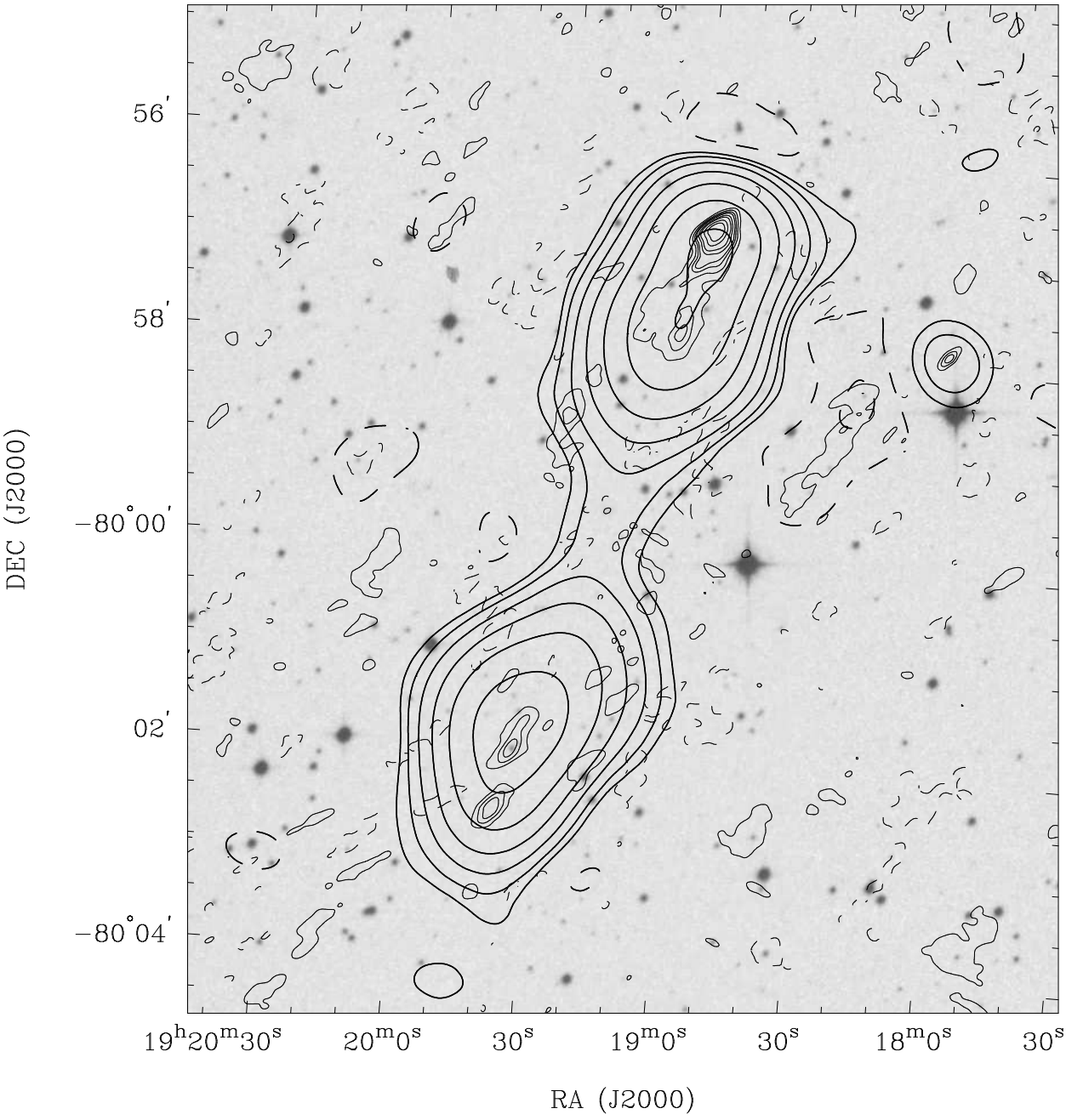

Fig. 16.— SGRS J1919−7959 radio contours on red SSS grey scale. SUMSS contours (thick lines) are at (−1, 1, 2, 4, 8, 16, 32, 64) × 4 mJy beam^{-1} and ATCA contours (thin lines) are at (−1, 1, 2, 3, 4, 6, 8, 12, 16) × 2 mJy beam^{-1}. The beams have FWHM 45.″7 × 45″ (SUMSS) and 11.″8 × 5.″1 (ATCA).

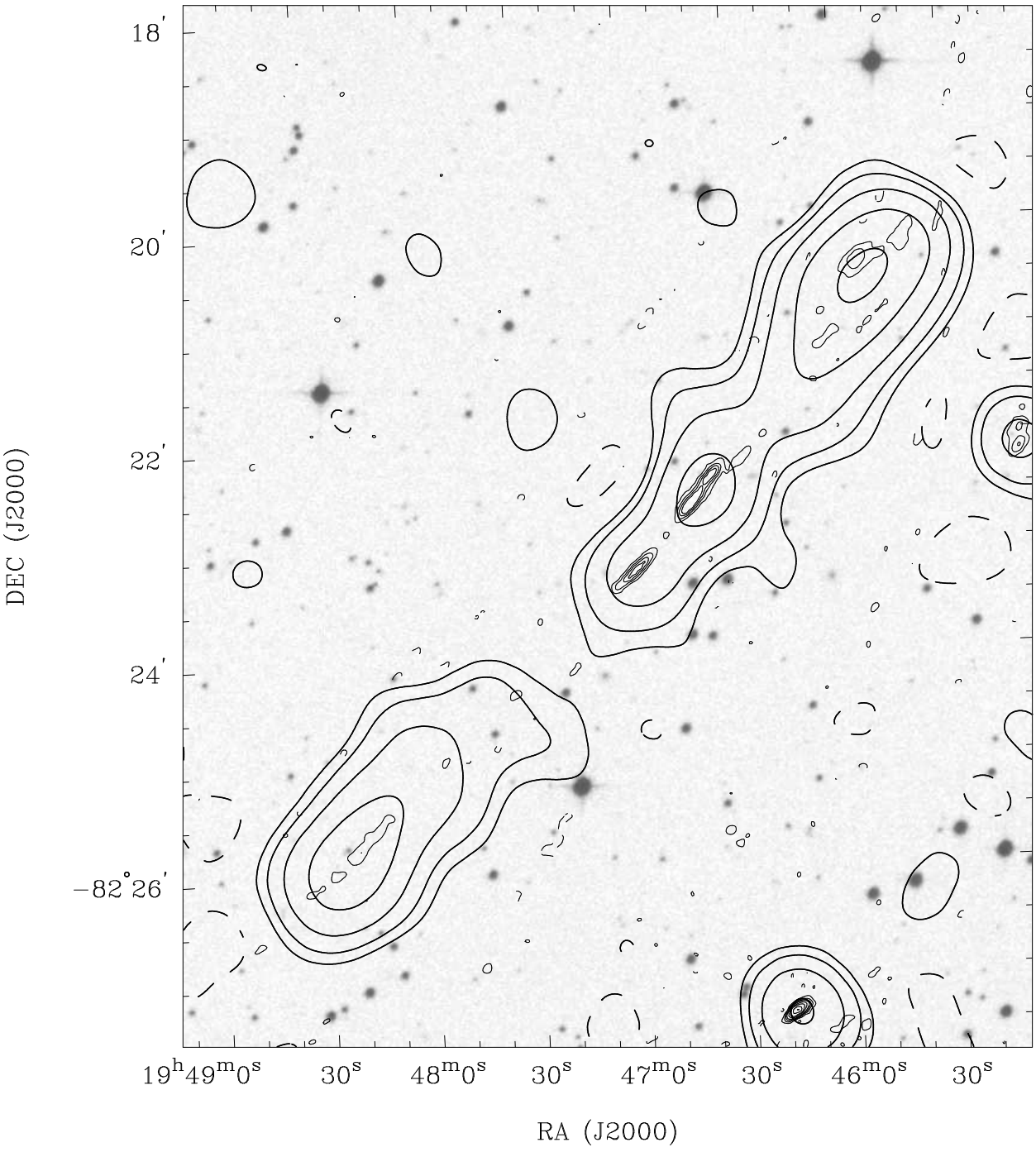

Fig. 17.— SGRS J1946−8222 radio contours on red SSS grey scale. SUMSS contours (thick lines) are at (−1, 1, 2, 4, 8, 16) × 2 mJy beam^{-1} and ATCA contours (thin lines) are at (−1, 1, 2, 3, 4, 6, 8, 12, 16) × 0.6 mJy beam^{-1}. The beams have FWHM 45.″2 × 45″ (SUMSS) and 10.″2 × 4.″3 (ATCA).

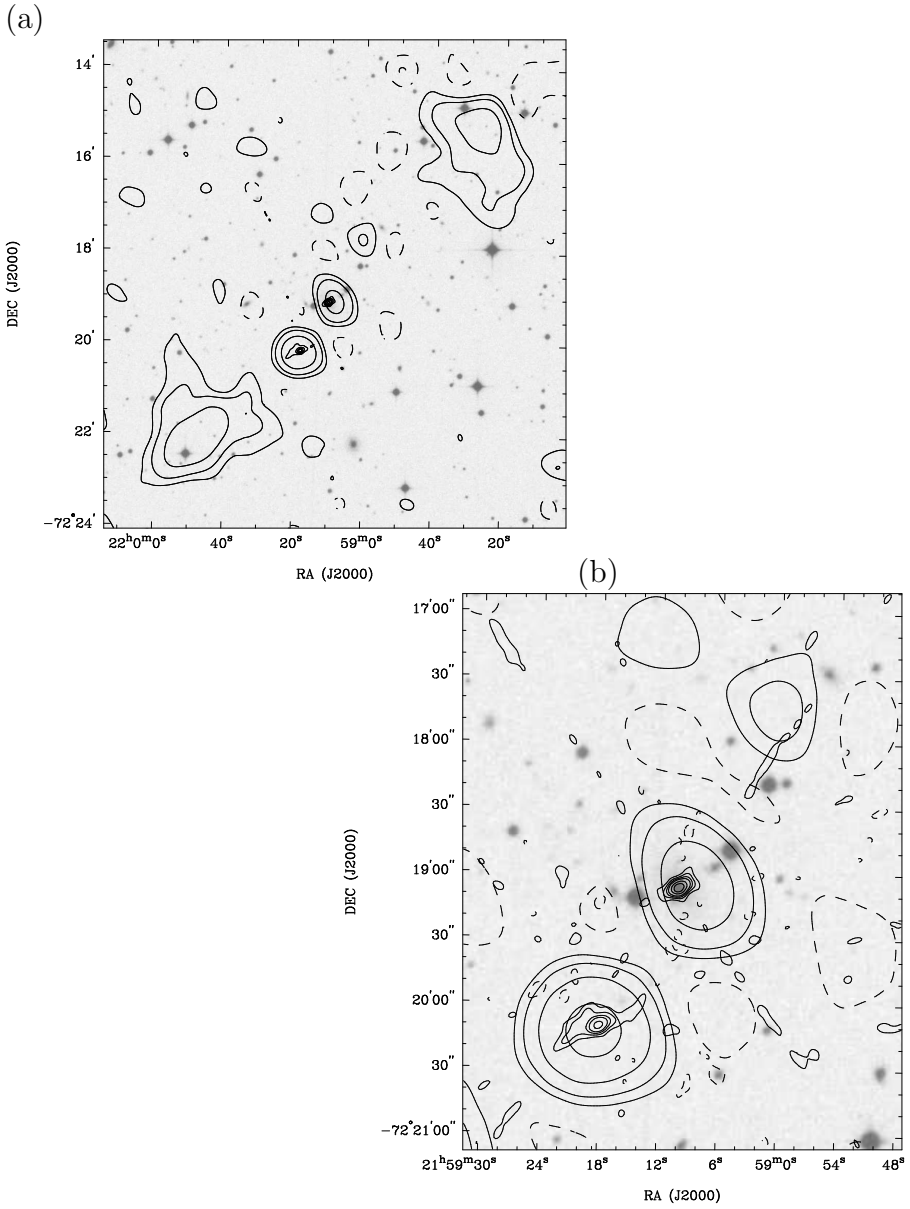

Fig. 18.— SGRS J2159−7219 radio contours on blue SSS grey scale. A zoom of the core region is shown in panel (b). SUMSS contours (thick lines) are at (−1, 1, 2, 4) × 2.5 mJy beam^{-1} and ATCA contours (thin lines) are at (−1, 1, 2, 3, 4, 6) × 1.5 mJy beam^{-1} in panel (a), In panel (b), SUMSS contours are at (−1, 1, 2, 4, 8) × 2 mJy beam^{-1} and ATCA contours are at (−1, 1, 2, 3, 4, 6, 8) × 1 mJy beam^{-1}. The beams have FWHM 47.″3 × 45″ (SUMSS) and 9.″4 × 6″ (ATCA).

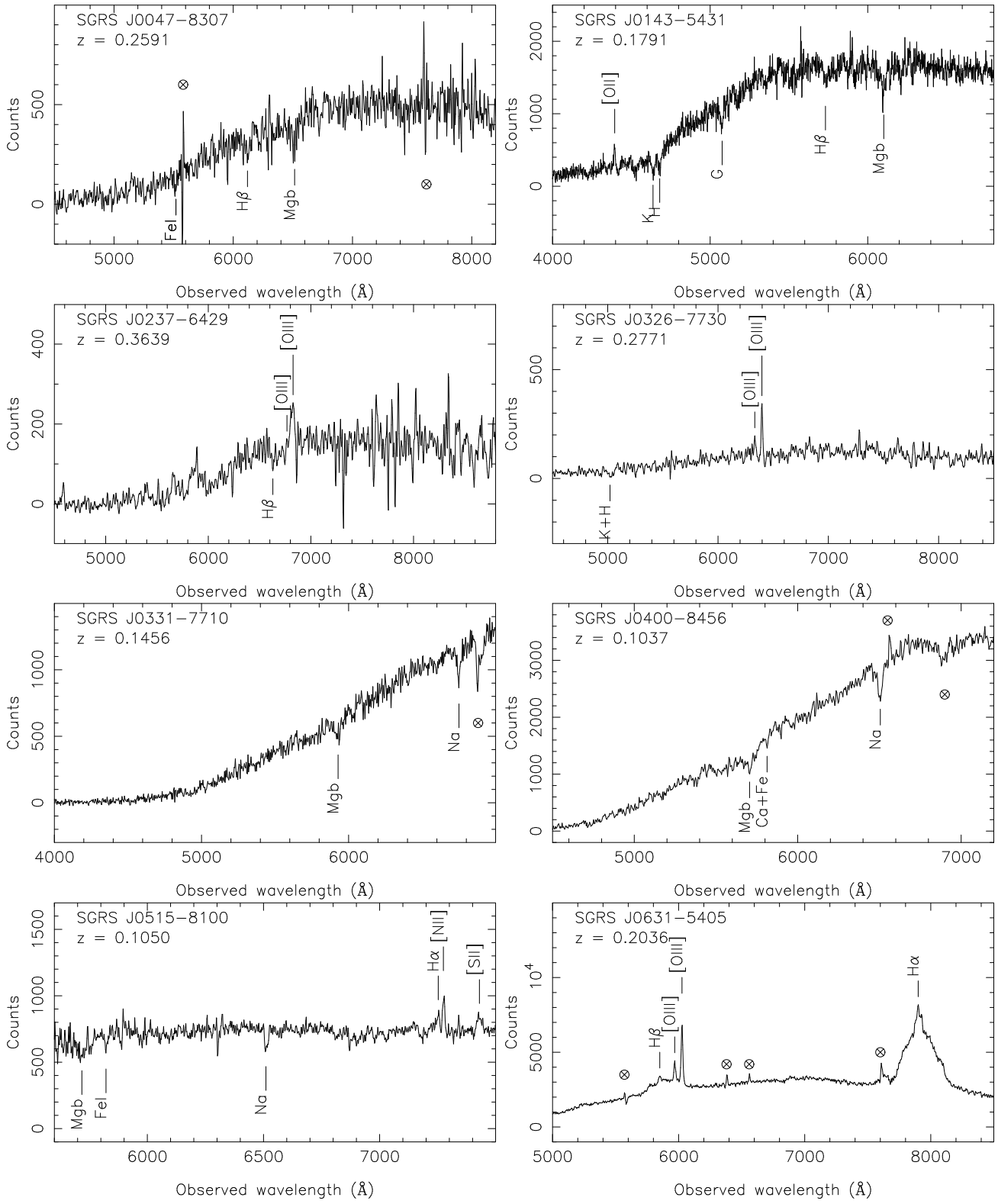

Fig. 19.— Optical spectra of the complete sample of giant radio sources. The symbol ⊗ represents features which we consider to be artifacts.

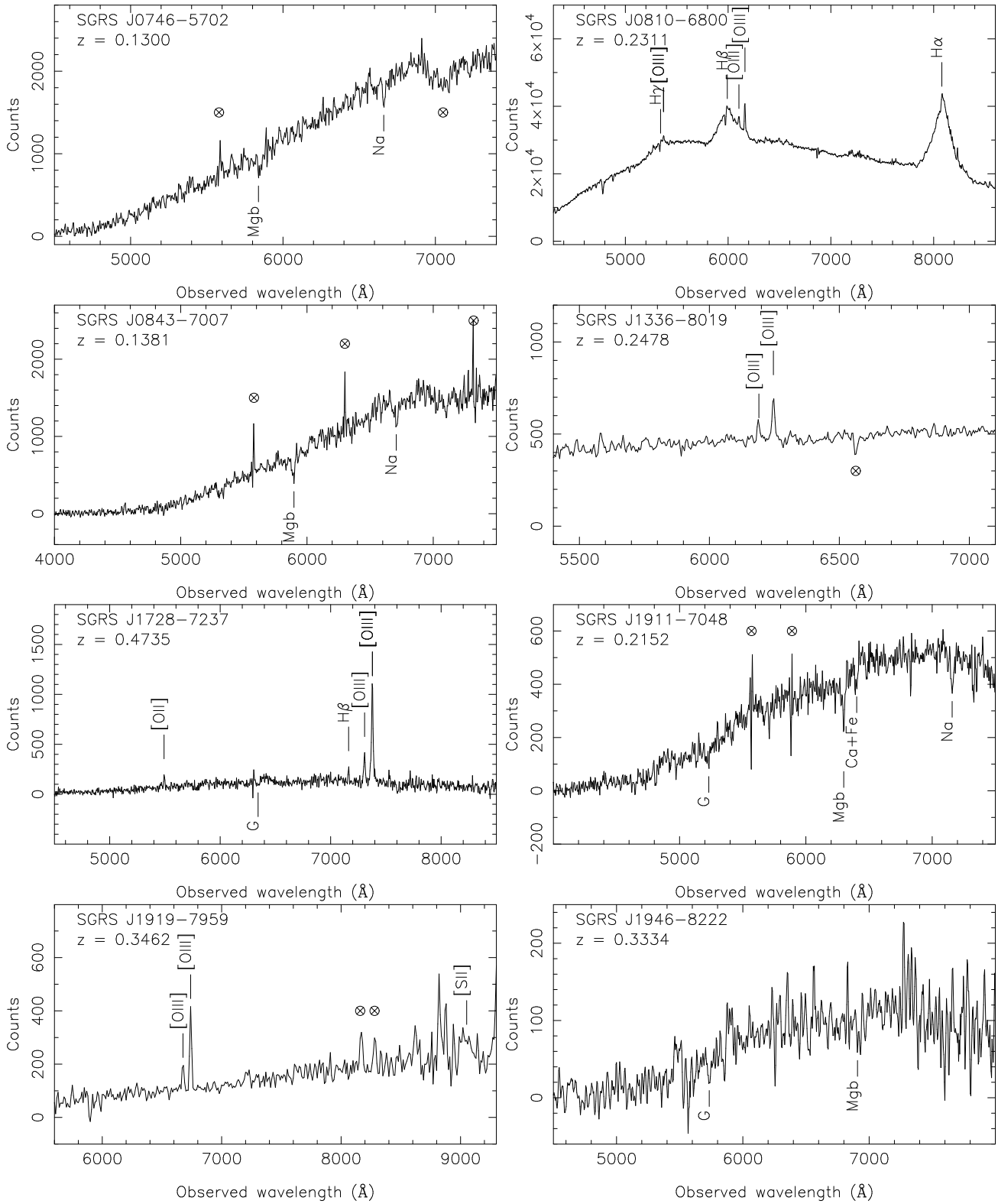

Fig. 19.— continued.

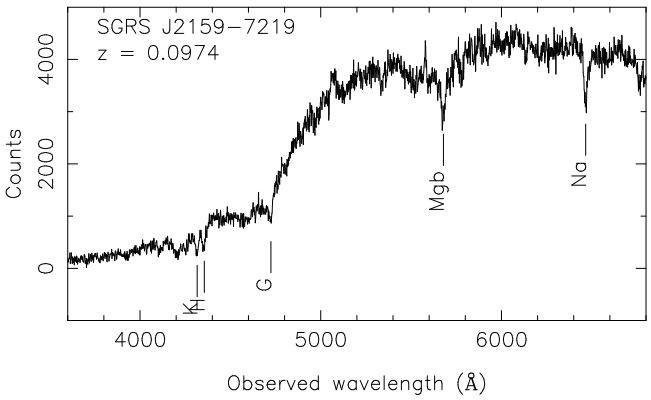

Fig. 19.— continued.

Table A1. Redshifts and spectral lines in spectra in Fig. 29

Name	Redshift	Prominent lines
SGRSC J0020−7321	0.0839±0.0001	Absorption lines: K, H, G, Hβ, Mgb, Na
SGRSC J0129−6433	0.1343±0.0002	Strong narrow emission lines: Hβ, [OIII]4959,5007, Hα+[NII] blend and [SII]6716,6731 Weak emission lines: Hγ+[OIII]4363, HeII4686 and [OI]6300
SGRSC J0414−6933	0.228:	Possible weak emission lines: Hα+[NII] blend and [SII]6716,6731. Absorption lines: Mgb and Na
SGRSC J2228−5600	0.0796±0.0002	Strong emission lines: [OIII]4959,5007, [OI] 6300, Hα+[NII] blend, [SII]6716,6731 Absorption lines: Mgb and Na
SGRSC J2336−8151	0.1190±0.0001	Absorption lines: K, H, G, Hβ, Mgb and Na

Table A2. Parameters for some of the rejected candidates

Name	Other names	SUMSS components	Redshift	Angular size (arcmin)	Type FR-I/FR-II	Linear size (Mpc)
SGRSC J0020−7321	PMN J0020−7321	J002046−732132	0.0839	4.8	FR-II	0.45
	PMN J0021−7322	J002021−732115				
		J002124−732219				
SGRSC J0129−6433	PMN J0129−6433	J012934−643353	0.1343	4.7	FR-II	0.66
		J012913−643223				
		J012941−643447				
SGRSC J0200−6007	PMN J0200−6007	J020019−600541	—	4.2	FR-II	—
		J020036−600825				
SGRSC J0414−6933	PMN J0414−6933	J041404−693407	0.228:	4.5	FR-II	0.98
		J041358−693552				
		J041414−693159				
SGRSC J1959−6402	PKS B1955−641	J195941−640420	—	4.9	FR-II	—
	PMN J1959−6403	J200007−640044				
	PMN J2000−6400					
SGRSC J2228−5600	PMN J2228−5559	J222753−560030	0.0796	4.8	FR-II	0.43
		J222823−555953				
		J222805−555950				
SGRSC J2253−5813	PMN J2253−5812	J225350−581319	—	4.3	FR-II	—
		J225411−581225				
SGRSC J2336−8151	PMN J2336−8151	J233607−815045	0.1190	5.4	FR-II	0.68
		J233816−815332				
		J233639−815139				

Table A3. Results of ATCA observations of the sources in Table A2

Name	Core positions	Flux density	
	RA & DEC (J2000 epoch)	1.4 GHz (mJy)	4.8 GHz (mJy)
SGRSC J0020−7321	00 20 43.3 −73 21 26.9	—	2.5
SGRSC J0129−6433	01 29 26.5 −64 33 36.0	3.9	
SGRSC J0200−6007	02 00 27.4 −60 07 04.9	2.3	
SGRSC J0414−6933	04 14 05.0 −69 34 11.5	12.9	
SGRSC J1959−6402	19 59 53.9 −64 02 36.1	4.3	
SGRSC J2228−5600	22 28 05.7 −55 59 48.2	40.2	
SGRSC J2253−5813	22 53 59.0 −58 12 49.8	5.4	
SGRSC J2336−8151	23 36 39.6 −81 51 41.2	9.4	

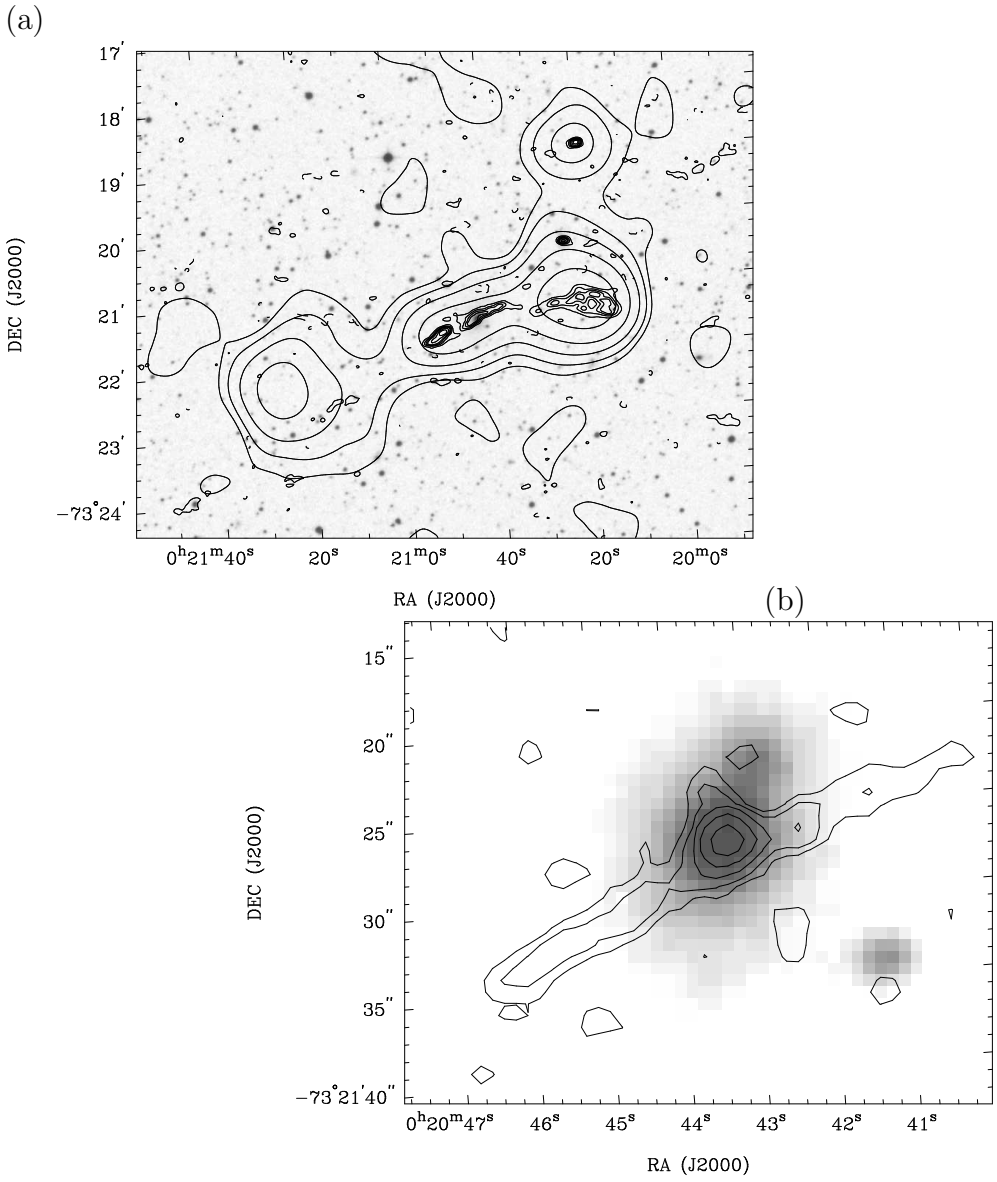

Fig. 20.— SGRSC J0020−7321 radio contours on red SSS optical grey scale image. ATCA 4.8-GHz image of the core is shown in the lower panel. SUMSS contours (thick lines) are drawn at (−1, 1, 2, 4, 8, 16) × 3 mJy beam^{-1}, ATCA contours (thin lines) are at (−1, 1, 2, 3, 4, 6, 8) × 0.5 mJy beam^{-1} (1.4 GHz) and at (−1, 1, 2, 3, 4, 6) × 0.1 mJy beam^{-1} (4.8 GHz). The beams have FWHM 47.″3 × 45″ (SUMSS), 7.″3 × 5.″2 (ATCA, 1.4 GHz) and 2.″1 × 1.″9 (ATCA, 4.8 GHz).

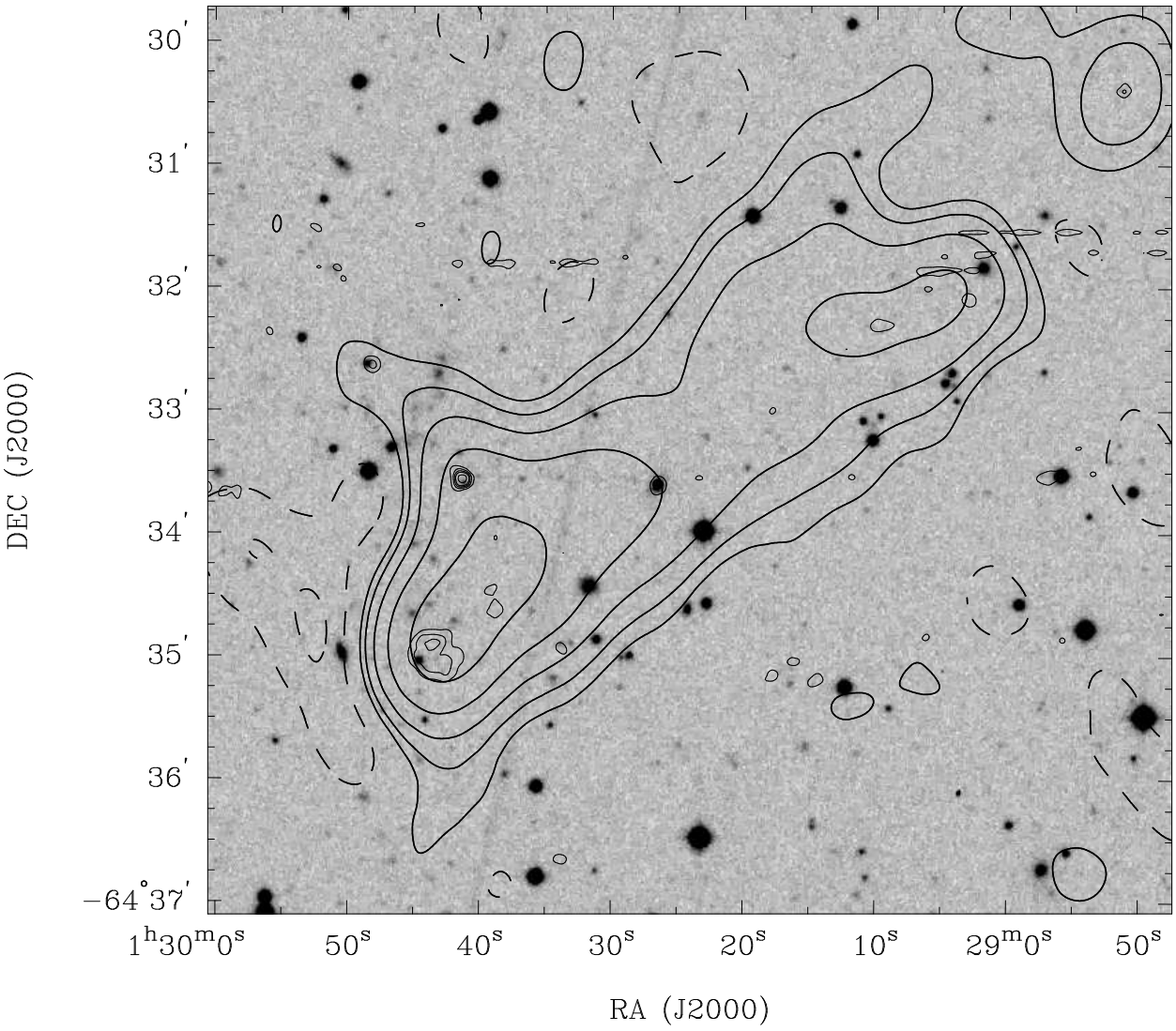

Fig. 21.— SGRSC J0129−6433 radio contours on blue SSS optical grey scale image. SUMSS contours (thick lines) are drawn at (−1, 1, 2, 4, 8, 16) × 3 mJy beam^{-1} and ATCA contours (thin lines) are at (1, 2, 3, 4, 6) × 0.8 mJy beam^{-1}. The beams have FWHM 50.″1 × 45″ (SUMSS) and 6.″5 × 5.″8 (ATCA).

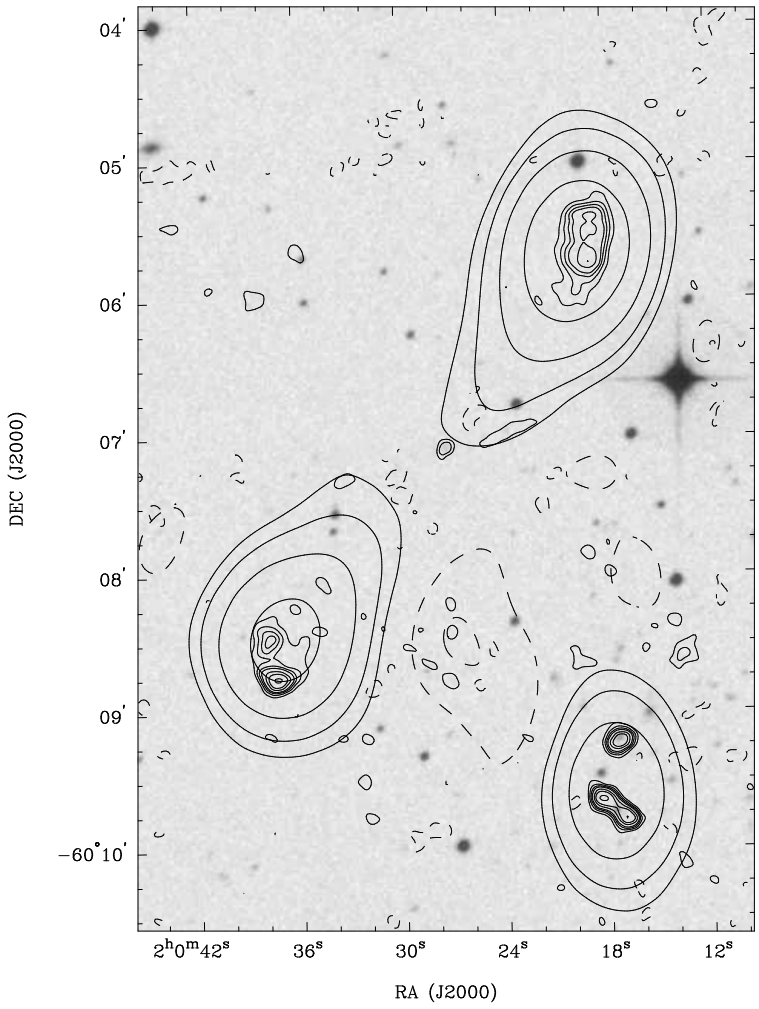

Fig. 22.— SGRSC J0200−6007 radio contours on blue SSS optical grey scale image. SUMSS contours (thick lines) are drawn at (−1, 1, 2, 4, 8) × 5 mJy beam^{-1} and ATCA contours (thin lines) are at (−1, 1, 2, 3, 4, 6, 8, 12) × 0.5 mJy beam^{-1}. The beams have FWHM 52″ × 45″ (SUMSS) and 6.″6 × 5.″9 (ATCA).

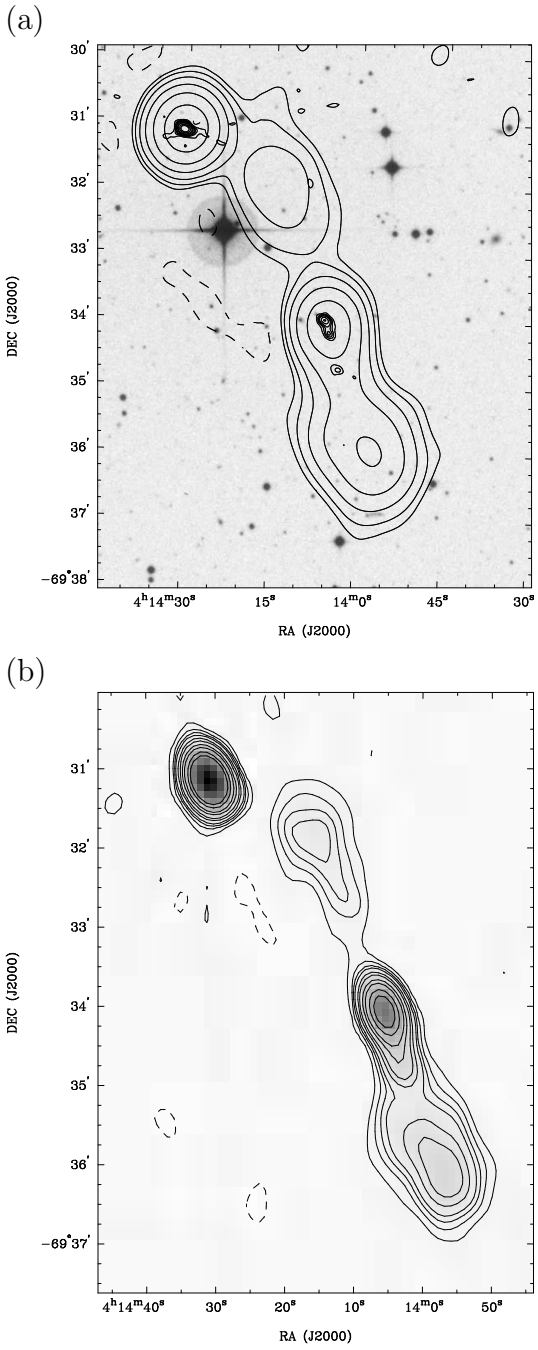

Fig. 23.— SGRSC J0414−6933 radio contours on blue SSS optical grey scale image. SUMSS contours (thick lines) are drawn at (−1, 1, 2, 4, 8, 16, 32) × 3 mJy beam^{-1}, ATCA contours (thin lines) are at (−1, 1, 2, 3, 4, 6, 8, 12, 16) × 3 mJy beam^{-1} (panel(a)) and (−2, −1, 1, 2, 3, 4, 6, 8, 12, 16, 24, 32) × 1.2 mJy beam^{-1} (panel (b)). The beams have FWHM 48.″5 × 45″ (SUMSS) and 9″ × 6.″2 (ATCA; panel (a)) and 32.″7 × 21.″5 (ATCA; panel (b)).

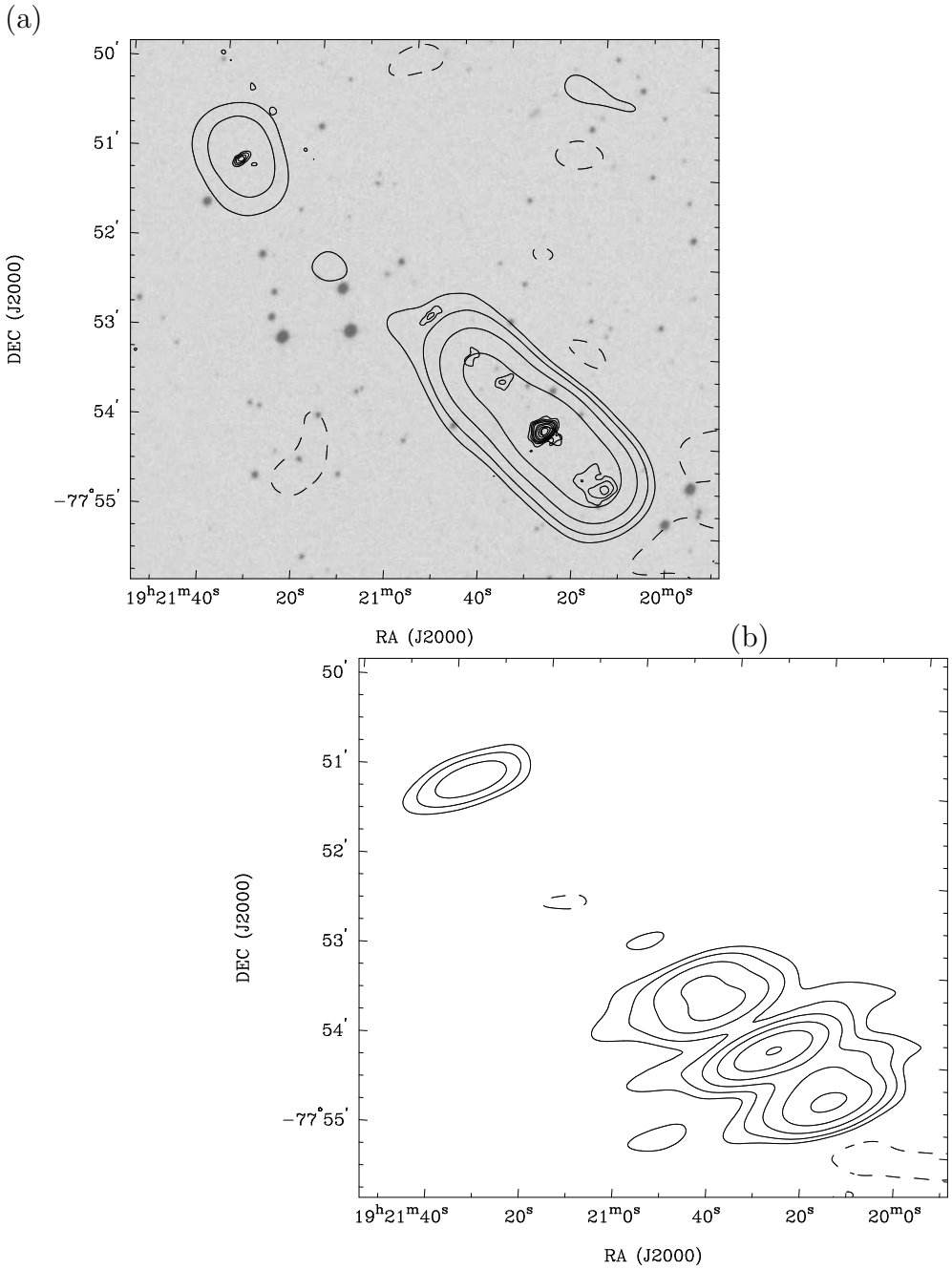

Fig. 24.— SGRSC J1920−7753 radio contours on red SSS optical grey scale image. SUMSS contours (thick lines) are drawn at (−1, 1, 2, 4, 8, 16) × 3 mJy beam^{-1} and ATCA contours (thin lines) are at (−1, 1, 2, 3, 4, 6, 8, 12, 16) × 0.8 mJy beam^{-1}. The beams have FWHM 46.″4 × 45″ (SUMSS) and 10.″3 × 4.″3 (ATCA). A 1.4-GHz ATCA image with a resolution of 52.″2 × 19″ is shown in the lower panel; contour levels are at (−1, 1, 2, 3, 4, 6, 8) × 0.8 mJy beam^{-1}.

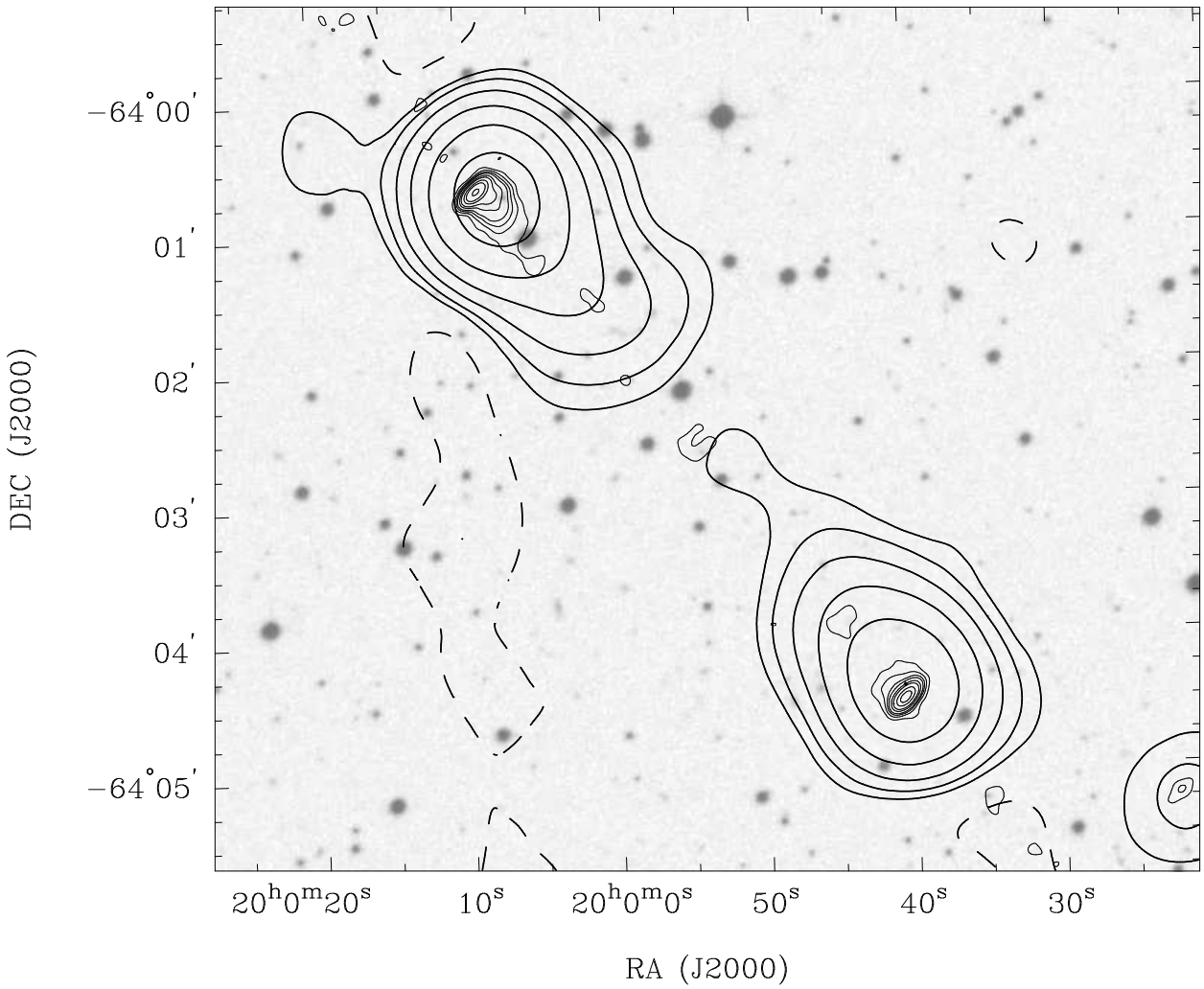

Fig. 25.— SGRSC J1959−6402 radio contours on red SSS optical grey scale image. SUMSS contours (thick lines) are drawn at (−1, 1, 2, 4, 8, 16, 32) × 5 mJy beam^{-1} and ATCA contours (thin lines) are at (−1, 1, 2, 3, 4, 6, 8, 12, 16, 24) × 3 mJy beam^{-1}. The beams have FWHM 50.″1 × 45″ (SUMSS) and 12.″2 × 5.″4 (ATCA).

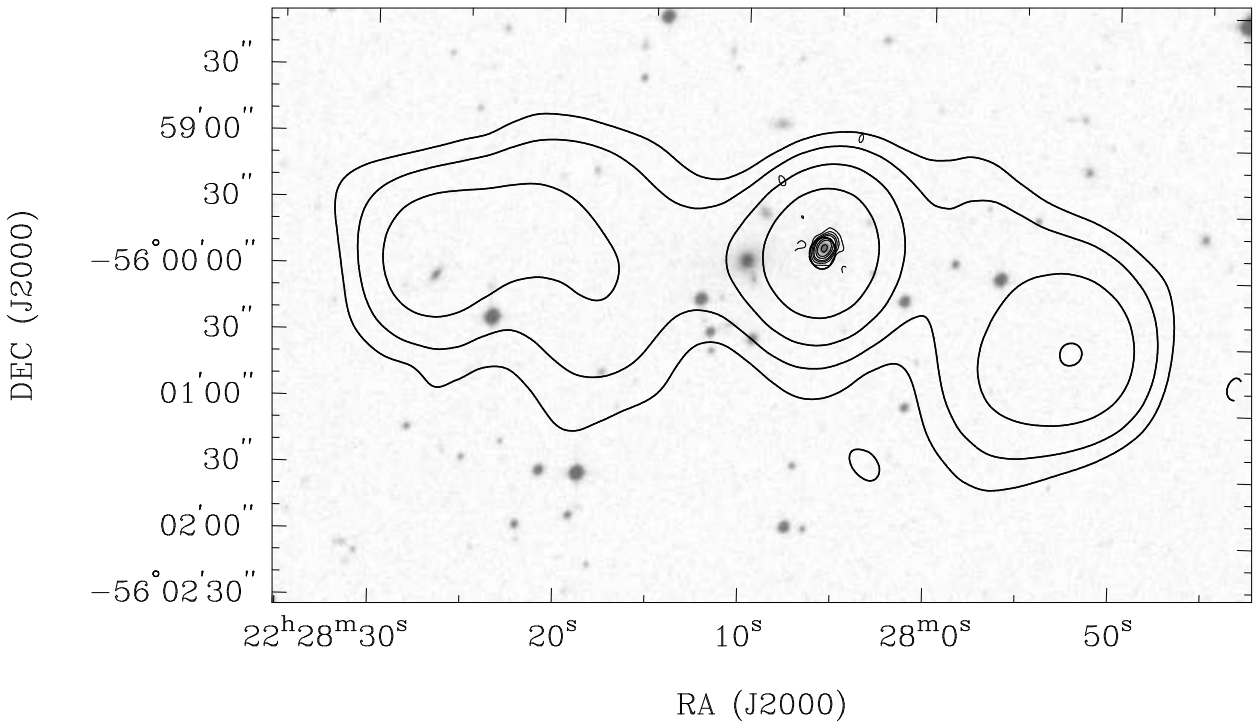

Fig. 26.— SGRSC J2228−5600 radio contours on blue SSS optical grey scale image. SUMSS contours (thick lines) are drawn at (−1, 1, 2, 4, 8, 16) × 3 mJy beam^{-1} and ATCA contours (thin lines) are at (−1, 1, 2, 3, 4, 6, 8, 12) × 3 mJy beam^{-1}. The beams used have a FWHM 54.″3 × 45″ (SUMSS) and 9.″3 × 6.″6 (ATCA).

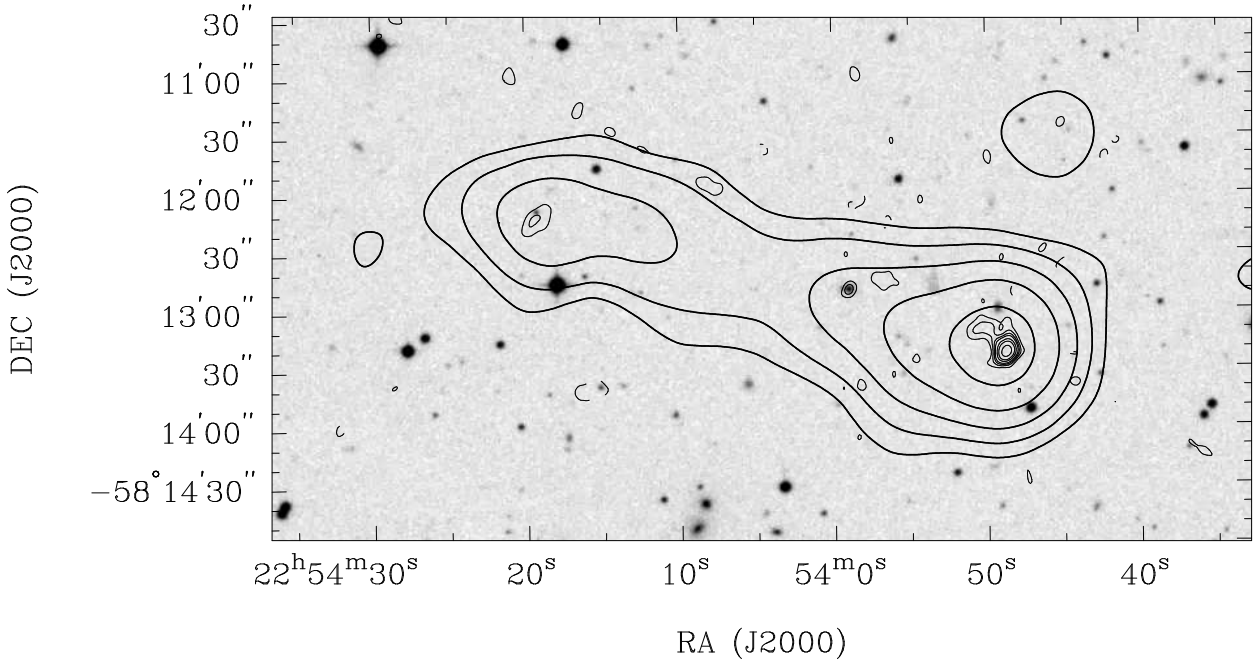

Fig. 27.— SGRSC J2253−5813 radio contours on blue SSS optical grey scale image. SUMSS contours (thick lines) are drawn at (−1, 1, 2, 4, 8, 16) × 4 mJy beam^{-1} and ATCA contours (thin lines) are at (−1, 1, 2, 3, 4, 6, 8, 12) × 2 mJy beam^{-1}. The beams have FWHM 52″ × 45″ (SUMSS) and 8.″9 × 6.″6 (ATCA).

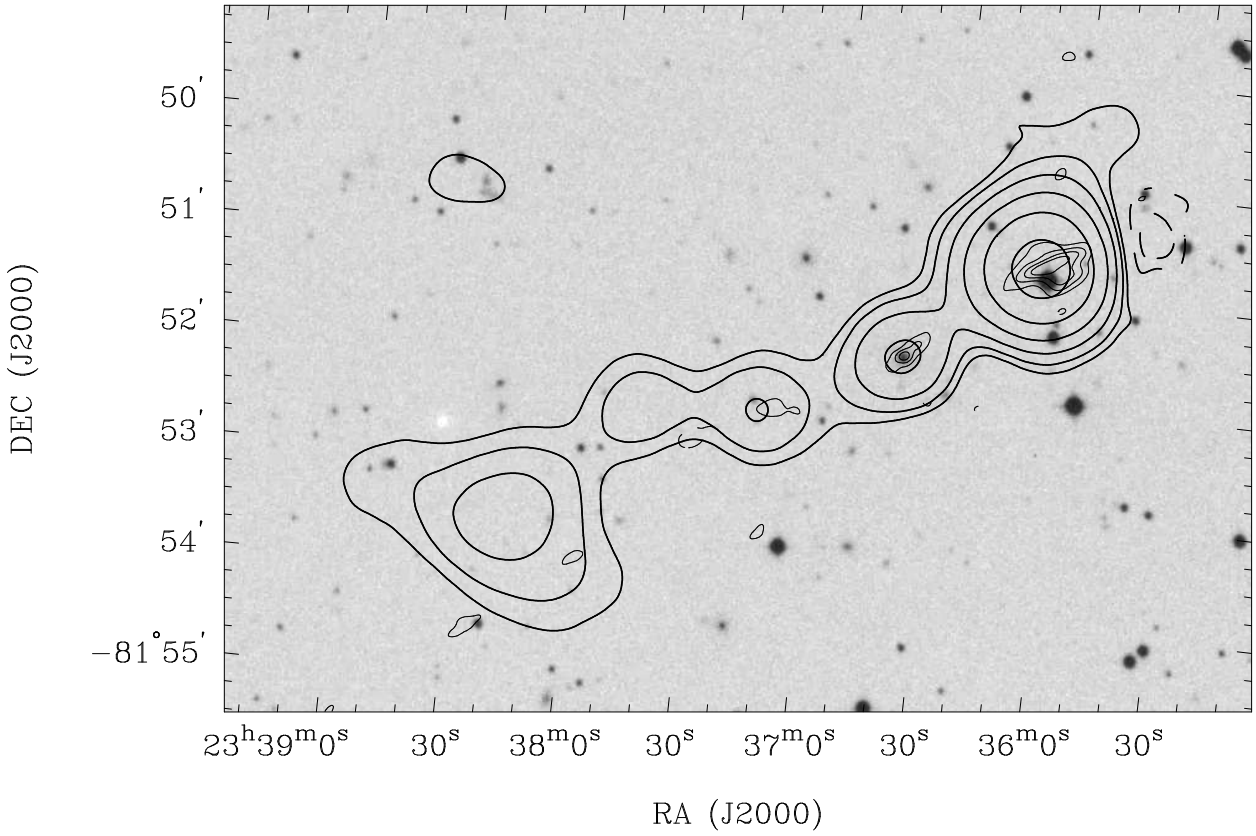

Fig. 28.— SGRSC J2336−8151 radio contours on blue SSS optical grey scale image. SUMSS contours (thick lines) are drawn at (−2, −1, 1, 2, 4, 8, 16, 32) × 4 mJy beam^{-1} and ATCA contours (thin lines) are at (−1, 1, 2, 3, 4) × 2.5 mJy beam^{-1}. The beams have FWHM 45.″7 × 45″ (SUMSS) and 8.″8 × 5.″9 (ATCA).

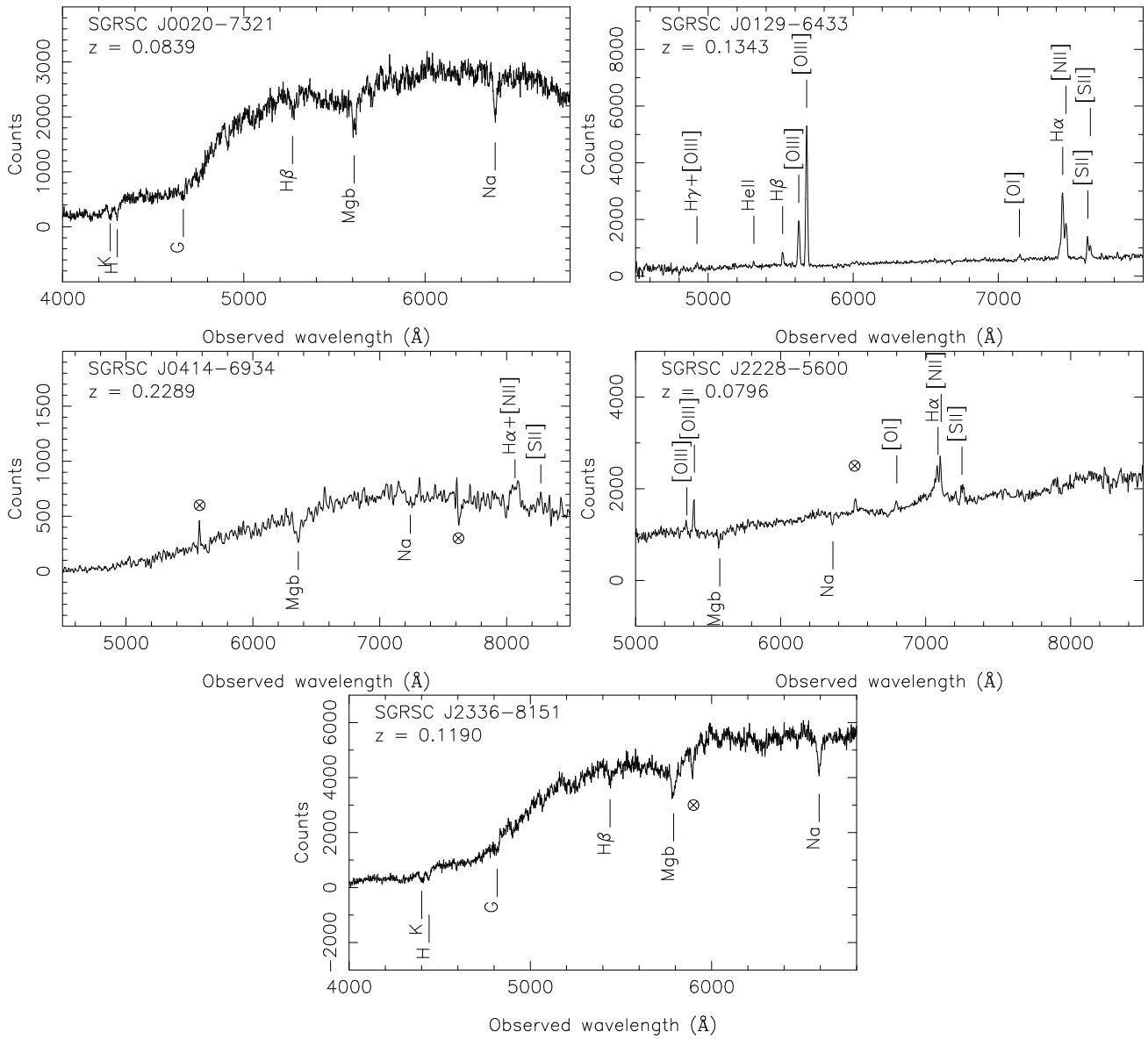

Fig. 29.— Optical spectra of the candidates that are not in the complete sample of giant radio sources.